Journal of Research of the National Bureau of Standards—D. Radio Propagation
Vol. 63D, No. 2, September–October 1959

Radio-Wave Scattering by Tropospheric Irregularities

Albert D. Wheelon [1]

(April 16, 1959)

The subject of radio-wave scattering by turbulent irregularities in the tropospheric index of refraction is reviewed. Descriptions of the turbulent medium are considered first, together with a status report on physical theories for the spectrum of irregularities. Phase and amplitude scintillations induced on electromagnetic waves propagated along line-of-sight paths are discussed next. The complementary problems of signal statistics and electromagnetic-propagation calculations are summarized and compared with available data. Both the geometrical optics and wave theory approaches are discussed. The theory of propagation beyond the horizon by scattering from the same irregularities is then described. A current review of the predictions for received power, signal fluctuations, and antenna effects is given. The paper is primarily a review of the essential and auxiliary predictions of scatter theory, but also contains a considerable amount of unpublished research by the author.

1. Introduction

The existence of random irregularities in the atmospheric index of refraction has been well established by direct measurements with microwave refractometers [1, 2].[2] The influence of these refractive irregularities on electromagnetic waves is confirmed by the random fading of microwave signals received beyond the optical horizon. Stochastic phase and amplitude variations imposed on electromagnetic waves propagated along line-of-sight paths confirm this cause-effect relationship. This is not to deny the influence of other mechanisms (layers, ducts, et al.) which may also contribute to scatter-field strengths. It *does* certify that the electromagnetically predicted relation between (turbulent) refractive variations and signal characteristics is indeed established.

The entire subject of electromagnetic propagation through turbulent refractive irregularities has received considerable theoretical and experimental attention during the post-war era. This attention is due to the enormous importance of "scatter propagation" communication systems on the one hand, and a basic limitation imposed on radio tracking and guidance systems for space vehicles on the other. The subject also has considerable scientific interest in its own right, particularly insofar as it unites electromagnetic theory, turbulence theory, and probability in an essential mixture. Once established, the influence of atmospheric irregularities on electromagnetic waves presents a valuable tool for studying turbulence at very large Reynolds numbers by simple radio means.

It now seems appropriate to try to establish how far the considerable volume of original research has brought the subject. This is particularly important since the basic concept is periodically brought under attacks of various sorts, and it is desirable to try to set forth the essential and auxiliary predictions of the basic theory in a coherent, unambiguous fashion. More important, however, is the need to present a balanced status report on the theoretical predictions, against which accumulating experimental results can be ranged to establish the true role of this mechanism in an objective manner.

The present paper is primarily a review of theoretical research on line-of-sight and scatter propagation in the United States, with a short status report on turbulence theories of atmospheric irregularities. It is not a genuine review, in that it leans rather heavily on the author's own research as a basis for unifying diverse results. Furthermore, a substantial amount of unpublished material is included herein. The report goes one step further and points out a number of outstanding problems which are solved in principle, but not in detail. A detailed, balanced comparison of these theoretical results with experimental data was not attempted for this broad field, although occasional references to significant results and prior comparisons are indicated by way of stimulating this crucial testing.

The substance of this report can be summarized briefly. In so far as the single scattering (Born) approximation and/or geometrical optics are valid representations of the electromagnetic response of propagating waves to refractive irregularities, the entire subject is solved in principle. The geometrical-propagation effects can be computed in any desired detail (or at least be reduced to integrals), independent of the turbulence model employed. This important separation is achieved by using the spectral representation for the space correlation of refractive irregularities, which allows any spectrum model to be combined with any propagation model. The more difficult electromagnetic problem of multiple scattering has not been considered adequately and is not discussed here.

[1] Consultant, Boulder Laboratories, NBS; permanent address, Space Technology Laboratories, Inc., Los Angeles 45, Calif.
[2] Figures in brackets indicate the literature references at the end of this paper.

2. Description of the Turbulent Medium

2.1. Statistical Characterization

The tropospheric index of refraction varies from point-to-point in a random manner. To describe this effect, one decomposes the dielectric constant ($\epsilon=n^2$) into its mean value and a small stochastic component.

$$\epsilon(\vec{r}, t)=\epsilon_0+\Delta\epsilon(\vec{r}, t). \tag{2.1.1}$$

It is this quantity which enters into the basic electromagnetic equations. ϵ_0 is usually a function of altitude (h) only, and its gradient appears in certain physical theories of turbulent irregularities. The stochastic function $\Delta\epsilon(\vec{r},t)$ is treated as a stationary, zero-mean random process in space and time, and is usually assumed to be spatially homogeneous and isotropic. If brackets denote ensemble, space, or time averages (which are equivalent for a statistically stationary, homogeneous atmosphere) the first two moments of $\Delta\epsilon$ are:

$$\langle\Delta\epsilon(\vec{r}, t)\rangle=0 \tag{2.1.2}$$

$$\langle\Delta\epsilon(\vec{r}, t)\overrightarrow{\Delta\epsilon(r+R, t)}\rangle=\langle\Delta\epsilon^2\rangle C(|\vec{R}|). \tag{2.1.3}$$

The intensity of dielectric fluctuations $\langle\Delta\epsilon^2\rangle$ is measured experimentally [1, 2] as several parts in 10^{-12}. The space-correlation function $C(R)$ falls to $1/e$ in a distance of several hundred feet, which is related to the scale length l_0 of the irregularities. Little attention has been paid to higher moments of $\Delta\epsilon$, except to note that they are completely specified in terms of $C(R)$ if the $\Delta\epsilon$ form a Gaussian random process.

2.2. Space Correlation Models

The space-correlation function $C(R)$ is the fundamental characterization of the turbulence. First-order propagation quantities depend upon integrals of $C(R)$, and one must assume an analytic model to perform the relevant calculations. The correlation must have the form

$$C(R)=f(R/l_0), \tag{2.2.1}$$

where $f(x)$ is the Fourier transform of a non-negative function. l_0 is called the scale length or average size of the blobs in the hierarchy of decaying eddies. The popular models for $f(x)$ are plotted together in figure 1.

1. *Bessel:* $f(x)=xK_1(x)$

This correlation model was devised to predict: (a) The observed linear-wavelength dependence of average power for tropospheric scatter propagation; and (b) certain features of line-of-sight propagation experiments. It has zero slope at the origin, and

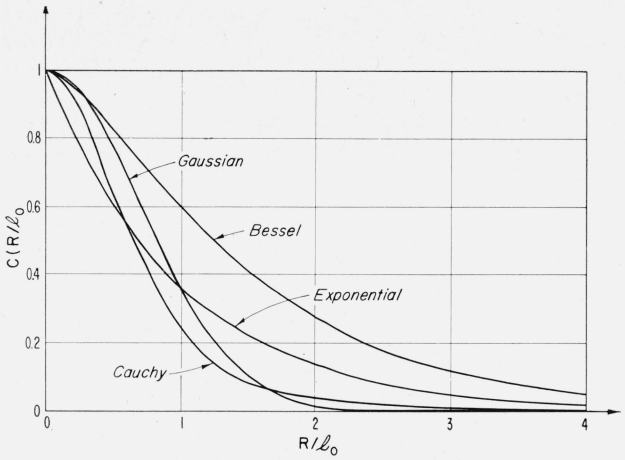

FIGURE 1.—*Plot of four common space correlation models for isotropic atmospheric irregularities.*

is suggested by the theory of turbulent mixing-in-gradient.

2. *Exponential:* $f(x)=e^{-x}$

This function has been widely used to study scatter propagation. However, its cusplike behavior (finite slope) at the origin implies infinite values for angle-of-arrival errors and other phase-derivative processes. The exponential model is possibly suggested by the physical theory of turbulent pressure fluctuations.

3. *Gaussian:* $f(x)=e^{-x^2}$

This is widely used for line-of-sight calculations because it can be integrated easily. It does not predict the results of tropospheric scatter experiments adequately and apparently has no foundation in physical theories of turbulence.

4. *Cauchy:* $f(x)=[1+x^2]^{-2}$

This model has been used for line-of-sight ray theory calculations, but is not founded in physical theories of turbulent irregularities.

It should be emphasized that any correlation function is only a model of the atmospheric irregularities, and must be carefully evaluated in terms of its ability to predict the results of experiments.

It is possible to generalize the foregoing to include anisotropic and inhomogeneous turbulent structures. Anisotropic irregularities can be described by introducing different scale lengths in orthogonal directions, viz,

$$C(R)=f\left(\left[\frac{x^2}{l_x^2}+\frac{y^2}{l_y^2}+\frac{z^2}{l_z^2}\right]^{1/2}\right), \tag{2.2.2}$$

and such effects are apparently relevant in the troposphere.

Refractometer experiments show that the intensity of dielectric fluctuations decreases with altitude [1]. One can describe an inhomogeneous field of this sort with a height-dependent $\langle\Delta\epsilon^2\rangle$ in eq (2.1.3), so long as the intensity does not change significantly in the several scale lengths l_0 required for the (space) averages.

A more difficult problem is encountered with the assumption of stationarity. There now seems to be experimental evidence [3] that the dielectric variations either: (1) do *not* form a stationary process; or (2) that there is a great deal of power in the low-frequency part of the spectrum of $\Delta\epsilon$, which appears as trend when viewed over a short span of time or space. Both explanations are probably partially correct, with a rapidly fading stationary process superimposed on long-period (diurnal, seasonal) harmonic components. Unfortunately, there is no adequate theory of nonstationary processes available to describe such effects.

2.3. Turbulence Spectrum Method

An equivalent characterization of a turbulent medium is given by the spectrum of irregularities $\vec{S}(\vec{k})$ [4, 5], which is the Fourier decomposition of the space correlation function,

$$\langle\Delta\epsilon^2\rangle\, C(\vec{R})=\frac{1}{8\pi^3}\int d^3k e^{-i\vec{k}\cdot\vec{R}}\vec{S}(\vec{k}). \qquad (2.3.1)$$

This representation has the advantge of exhibiting an explicit R-dependence for the correlation without committing the study to a particular turbulence model. Propagation calculations can be performed on the generic term $\exp[-i\vec{k}\cdot\vec{R}]$ by reversing the orders of integration. The physics of the atmospheric irregularities re-enters the problem eventually in the spectrum $\vec{S}(\vec{k})$, which must be introduced to complete the wavenumber (k) integration. If the medium is isotropic, $\vec{S}(\vec{k})$ depends only on $|\vec{k}|$, and the space correlation becomes:

$$\langle\Delta\epsilon^2\rangle C(R)=\frac{1}{2\pi^2}\int_0^\infty dk k S(k)\,\frac{\sin kR}{R}. \qquad (2.3.2)$$

The mean square fluctuation at a point,

$$\langle\Delta\epsilon^2\rangle=\frac{1}{2\pi^2}\int_0^\infty dk k^2 S(k), \qquad (2.3.3)$$

indicates that the spectrum represents the ability of each blob-size group (wavenumber range) to produce irregularities.

Equation (2.3.1) may be inverted to establish the spectrum which corresponds to each of the correlation functions discussed earlier. Table 1 indicates the spectra for the Bessel, Exponential, Gaussian and Cauchy models. The small R behavior of the correlation is determined by the large k range of the spectrum and vice versa.

TABLE 1. *Correspondence of turbulence spectrum and space correlation functions for several models of atmospheric irregularities*

	Bessel	Exponential	Gaussian	Cauchy
Space correlation $C(R)$	$\frac{R}{l_0}K_1\left(\frac{R}{l_0}\right)$	e^{-R/l_0}	e^{-R^2/l_0^2}	$\left[1+\frac{R^2}{l_0^2}\right]^{-2}$
Turbulence spectrum $S(k)$	$6\pi^2\frac{\langle\Delta\epsilon^2\rangle l_0^3}{[1+k^2l_0^2]^{5/2}}$	$8\pi\frac{\langle\Delta\epsilon^2\rangle l_0^3}{[1+k^2l_0^2]^2}$	$\pi^{3/2}\langle\Delta\epsilon^2\rangle l_0^3 e^{\frac{-k^2l_0^2}{4}}$	$\pi^2\langle\Delta\epsilon^2\rangle l_0^3 e^{-kl_0}$

2.4. Physical Theories of Dielectric Irregularities

The index of refraction in the (nonionized) troposphere and stratosphere is independent of radio-frequency from 10 to 10,000 Mc. Variations of the refractive index from unity are measured as several hundred parts per million, and are related to standard meteorological parameters by the empirical formula:

$$n-1=\left\{77.6\frac{P}{T}+3.73\times10^5\frac{e}{T^2}\right\}10^{-6} \qquad (2.4.1)$$

where

T = air temperature is degrees Kelvin (absolute),
P = total air pressure in millibars, and
e = partial water-vapor pressure in millibars.

Dielectric variations ($\epsilon=n^2$) are thus related to temperature, pressure and water-vapor fluctuations by

$$\Delta\epsilon=2\times10^{-6}\left\{\begin{array}{l}-\Delta T\left(77.6\frac{P}{T^2}+7.46\times10^5\frac{e}{T^3}\right)\\ +\Delta P\left(\frac{77.6}{T}\right)+\Delta e\left(\frac{3.73\times10^5}{T^2}\right)\end{array}\right\} \qquad (2.4.2)$$

Dielectric variations in the lower troposphere are governed principally by water-vapor irregularities, and one is dealing with the irregularities established in a passive scalar by turbulent movements of the random atmospheric velocity field. This process is characterized by the turbulent mixing theories described below.

In the stratosphere there is a negligible amount of water vapor, and dielectric variations are produced almost exclusively by thermodynamic fluctuations: ΔT and ΔP. The primary mechanism for producing irregularities in the stratosphere is also probably turbulent mixing by rotating eddies. However, one must now recognize thermodynamic expansion (perhaps adiabatic [6]) of the gas as the eddies transfer parcels of air between different altitude levels, corresponding to different ambient temperatures and pressures. This expansion correction is not dominant in the lower troposphere, but probably plays a central role in the propagation of scatter signals to distances greater than 700 km by common volume elements in the stratosphere [6].

The spectrum method makes direct contact with physical theories or turbulent irregularities which predict $S(k)$ in certain wavenumber ranges. These theories identify three distinct ranges of the spectrum, as shown in figure 2.

1. $0<k<k_0$: The input or blob-creating range corresponds to very large scale lengths, which are probably anisotropic. The upper end, k_0, of this

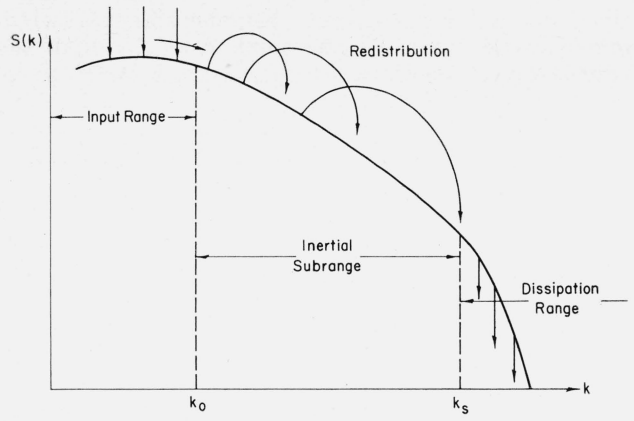

FIGURE 2.—*Typical spectrum of dielectric irregularities plotted versus wavenumber, showing various turbulence ranges.*

range is approximately the reciprocal of the correlation or scale length l_0 discussed earlier, which is of the order of 100 m in the troposphere. Since we do *not* know (in detail) how turbulence is created from a laminar flow, turbulence theories carefully avoid this range. It is important to note that the spectra listed in table 1 *do* make definite statements about this range, so the large R behavior of the corresponding correlation models must be regarded as extrapolation or pure guesswork.

2. $k_0<k<k_s$: The inertial subrange is characterized by redistribution of the turbulent "energy" toward higher wavenumbers and represents the progressive subdivision of eddies in the turbulent structure. Dimensional analysis can be used here with considerable confidence. Tropospheric-scatter propagation depends principally on this inertial range.

3. $k_s<k<\infty$: The dissipation range is characterized by a sharp drop in turbulent activity, due to the destructive action of viscosity and diffusion. In the troposphere, $l_s=k_s^{-1}$ is of the order of millimeters. We do not consider the dissipation range, since aperture and recorder smoothing effectively eliminate the contributions of such tiny blobs in the troposphere.[3]

Three turbulence theories have been developed which predict $S(k)$ in the inertial range:

a. Pressure Fluctuations

Fluctuations of the velocity field induce pressure variations according to Bernoulli's law. If variation of pressure, density, and water-vapor content are related linearly, the spectrum of dielectric fluctuations is given by [7],

$$S(k)=\left(\frac{v_0}{c}\right)^4 \frac{k_0^{4/3}}{k^{13/3}},\ (k>k_0) \tag{2.4.3}$$

where v_0 is the speed of the largest blobs and c the local speed of sound. Most writers now agree that this mechanism is unimportant for the lower troposphere [8].

b. Obukhov's Mixing Theory

In this theory, an external source is imagined to feed fluctuations into the spectrum at the largest size (k_0). Subsequent redistribution down the inertial range is attributed to turbulent convection, for which dimensional arguments give [9, 10, 11]

$$S(k)=\langle\Delta\epsilon^2\rangle \frac{k_0^{2/3}}{k^{11/3}},\ (k>k_0). \tag{2.4.4}$$

If the external source is identified only with the mixing of a gradient by the largest blobs, the intensity is given by

$$\langle\Delta\epsilon^2\rangle=k_0^{-2}\left(\frac{d\epsilon_0}{dh}\right)^2; \tag{2.4.5}$$

which is supplied at the input wavenumber k_0. Adiabatic expansions of the mixing eddies modify the ambient gradient in the stratosphere [6].

c. Mixing-in-Gradient Theory

This approach considers an initial refractive-index gradient and how it is changed by turbulent convection at *all* wavenumbers. The rotating turbulent eddies transfer parcels of water vapor from low to high points on the profile and vice versa, and establish irregular contrasts thereby. The mechanism for turbulent fluctuations appears explicitly in this theory at all wavenumbers and no external source is required. The inertial range is again amenable to unambiguous dimensional arguments [8, 12].

$$S(k)=\left(\frac{d\epsilon_0}{dh}\right)^2 \frac{1}{k^5},\qquad (k>k_0) \tag{2.4.6}$$

and the result is independent of turbulent parameters, except for restrictions on its range of validity. Adiabatic expansions of the eddies are again important in the stratosphere [6]. In the range $k>k_0$, we see that this model agrees with the spectrum computed from the Bessel space-correlation model indicated in table 1.

Both of the mixing theories predict that the intensity of turbulent fluctuations should be proportional to the local gradient of the inhomogeneous mean profile. A good correlation between the strength of scatter signals and the monthly mean refractive gradient has been observed experimentally on many paths [13]. Since strong scattered signals are associated with large dielectric fluctuations, this must be considered an important success for the gradient-dependent mixing mechanisms. On the other hand, observed absences of dielectric irregularities at inversion layers and other stable meteorological interfaces suggests that the mixing-in-gradient models may not be applicable to very sharp gradients.

[3] The dissipation is apparently quite important for ionospheric-scatter propagation at vhf.

2.5. Space-Time Correlations of Irregularities

The averaged product of two dielectric fluctuations taken at different positions and times is of considerable importance in studying the time variability of signal amplitude and phase for both line-of-sight and beyond-the-horizon propagation.

$$\langle \Delta\epsilon(\vec{r},t)\Delta\epsilon(\overrightarrow{r+R},t+\tau)\rangle = \langle \Delta\epsilon^2\rangle C(\vec{R},\tau) \quad (2.5.1)$$

Temporal variations of $\Delta\epsilon$ are associated with motion of the carrier medium, and two distinct types of atmospheric motion are important:

a. Drifting Convection

A prevailing wind with constant velocity $\vec{U}$ would bear a frozen turbulent structure along intact and would translate the entire structure a distance $\vec{U}\,\tau$ in a time τ. Since the atmosphere is assumed to be homogeneous, this would be just the same as measuring the space correlation between irregularities separated by a distance of $\vec{U}\,\tau$ at the same time.

b. Random Motion

The random motion associated with the continuous eddy-breakup process rearranges the turbulent irregularities in time. This self-motion effect is probably isotropic for small (k) scale irregularities. The random motion would be apparent even if there were no drift velocity, or if one rode along on the prevailing winds.

The spectrum method is particularly well-suited to describing the combined effect of these two motions, in that their effects can be explicitly separated in the integrand of the wavenumber integral representation of the space-time correlation [4, 14].

$$\langle \Delta\epsilon(\vec{r},t)\Delta\epsilon(\overrightarrow{r+R},t+\tau)\rangle = \frac{1}{8\pi^3}\int d^3k S(\vec{k}) e^{i\vec{k}\cdot(\overrightarrow{R+U\tau})}\eta(\vec{k},\tau) \quad (2.5.2)$$

For an isotropic spectrum of irregularities, this becomes:

$$\langle \Delta\epsilon(\vec{r},t)\Delta\epsilon(\overrightarrow{r+R},t+\tau)\rangle = \frac{1}{2\pi^2}\int_0^\infty dk k^2 S(k)\,\frac{\sin\,(k|\overrightarrow{R+U\tau}|)}{|\overrightarrow{R+U\tau}|}\,\eta(k,\tau). \quad (2.5.3)$$

The function $\eta(k,\tau)$ describes the time autocorrelation of fluctuations contained in a fixed wavenumber interval k, and is unity for zero time displacement τ. Dimensional turbulence arguments indicate that $\eta(k,\tau)$ should depend only on the product[4] $V_0 k_0^{1/3} k^{2/3}\tau$ in the inertial subrange [15, 16], although no functional dependence has yet been established. However, detailed studies of the turbulent velocity field-time correlations over the entire spectrum indicate that the coefficient of τ varies from $k^{2/3}$ to k [17].

Convective motion is probably the dominant effect for line-of-sight propagation, since eddy speeds V_0 are usually much less than the prevailing wind speed U.[5] However, scatter propagation geometry discriminates against a horizontal drift velocity at the path midpoint and Doppler shifts introduced by the random motion can dominate.

3. Line-of-Sight Propagation

3.1. Introduction

Phase and amplitude instability on line-of-sight propagation paths is important in practice because of the limitations it imposes on interferometric tracking schemes and frequency synchronization operations. Before launching into detailed discussions of problems, it is well to examine the two principal geometrical situations shown in figure 3. These problems are idealized by omission of ground reflections, which are ignored since they do not contribute scintillations unless moving foliage or water surfaces are a major factor.

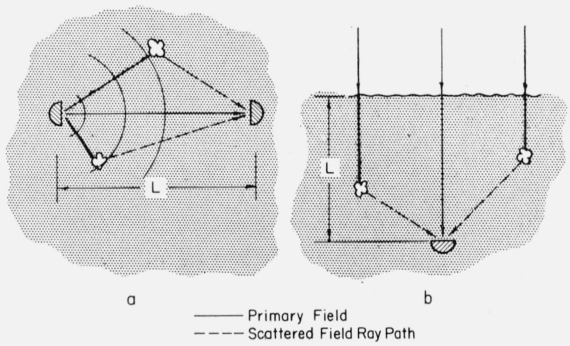

FIGURE 3.—*Typical ray paths for idealized line-of-sight problems: (a) Relay link immersed in an infinite turbulent medium, and (b) radio star viewed vertically through a turbulent mantel.*

a. Relay Link Problem

Receiver and transmitter are both immersed in an infinite turbulent region a distance L apart. The transmitter emits spherical waves and the receiver is also assumed to be omnidirectional.

b. Radio Star Problem

Plane waves are assumed to fall on a semi-infinite turbulent medium with the receiver located a distance L below the upper boundary. The turbulence may be graduated toward its upper boundary by

[4] V_0 and k_0 are the speed and wavenumber at the input stage of the turbulent velocity spectrum.

[5] Since the turbulent velocity field itself is a (small) partition of the kinetic energy in the laminar (drift) field.

using an inhomogeneous turbulence intensity $\langle \Delta\epsilon^2(r) \rangle$.

It is significant that the receiver always stands in the (tropospheric) turbulent medium for line-of-sight propagation, and blobs which are just on top of the receiver play an important role.

3.2. Signal Statistics and Vector Voltage Diagrams

The typical ray-path trajectories shown in figure 3 indicate that the field which falls on the receiver is composed of two terms: (a) The unperturbed primary field E_0 propagated along the line-of-sight, and (b) the incoherent superposition of waves scattered to the receiver by all volume elements in the scattering region V. The primary field induces a constant voltage A_0 in the receiver, which serves as a convenient phase reference. Because of the randomly varying multipath combinations, the total scattered wave induces statistical signal components $x(t)$ and $y(t)$ which are in and out-of-phase with respect to the constant vector A_0, as shown in the vector voltage diagrams of figure 4. Experiments measure the composite amplitude A and the relative phase excursions α about the phase reference A_0. A typical phase record is shown in figure 4, together with the vector voltage diagrams appropriate to two displaced times t_1 and t_2.

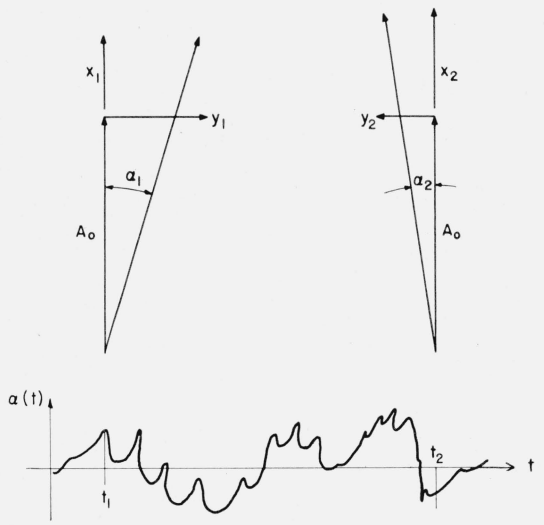

FIGURE 4.—*Typical phase record of randomly-varying line-of-sight signal showing the corresponding time-displaced vector voltage diagrams for a constant signal plus noise.*

The basic statistical problem is to estimate the probability distributions for amplitude A and phase α, and from these the relevant statistical estimates of the randomly varying quantities. Since the orthogonal signal components $x(t)$ and $y(t)$ are induced by the scattering contributions from many independent blobs, they may be characterized by a Gaussian distribution according to the Central Limit Theorem.

$$P[x,y]\,dx\,dy = \frac{dx\,dy}{2\pi\sigma_x\sigma_y}\,\frac{1}{\sqrt{1-\rho^2}}\exp-\left[\frac{\frac{x^2}{\sigma_x^2}+\frac{y^2}{\sigma_y^2}-\frac{2\rho xy}{\sigma_x\sigma_y}}{2(1-\rho^2)}\right]. \tag{3.1.1}$$

The moment parameters,

$$\langle x^2\rangle=\sigma_x^2,\ \langle y^2\rangle=\sigma_y^2,\ \langle xy\rangle=\sigma_x\sigma_y\rho$$

should be determined from explicit propagation calculations. Previous statistical discussions have *assumed*,

$$\sigma_x^2=\sigma_y^2=\sigma^2, \text{ and } \rho=0, \tag{3.1.2}$$

in order to simplify the analysis. We should like to point out, however, that such assumptions are not in agreement with available propagation calculations, which suggest rather that

$$\sigma_x^2+\sigma_y^2=\text{constant},\ \rho \text{ finite}. \tag{3.1.3}$$

A new effort on the statistical problem is required for propagation work.

For present purposes, we simply review available results derived on the assumptions (3.1.2). If the (A_0) displaced cylindrical coordinates of figure 4 are inserted into eq (3.1.1), the joint amplitude-phase distribution becomes:

$$P(A,\alpha)dAd\alpha=\frac{AdAd\alpha}{2\pi\sigma^2}\exp -\left\{\frac{A^2+A_0^2-2AA_0\cos\alpha}{2\sigma^2}\right\} \tag{3.1.4}$$

The distribution of total voltage amplitudes A was established by Rice [18] from (3.1.4) by integrating the phase α from $-\pi$ to π.

$$P(A)dA=\frac{AdA}{\sigma_2}\,I_0\left(\frac{AA_0}{\sigma_2}\right)\exp-\left[\frac{A^2+A_0^2}{2\sigma^2}\right]. \tag{3.1.5}$$

From this expression one can calculate the amplitude moments.

$$\langle A\rangle=\sqrt{\frac{\pi}{2}}\,\sigma e^{-A_0^2/4\sigma^2}\left[\left(1+\frac{A_0^2}{2\sigma^2}\right)I_0\left(\frac{A_0^2}{4\sigma^2}\right)+\left(\frac{A_0^2}{2\sigma^2}\right)I_1\left(\frac{A_0^2}{4\sigma^2}\right)\right] \tag{3.1.6}$$

and

$$\langle A^2\rangle=A_0^2+2\sigma^2 \tag{3.1.7}$$

The probability that the amplitude exceeds a prescribed level a is obtained by integrating (3.1.5) from a to ∞. Numerical tables of this probability have been prepared [19] and are reproduced on Rayleigh graph paper in figure 5. The addition of a constant vector evidently increases the average signal

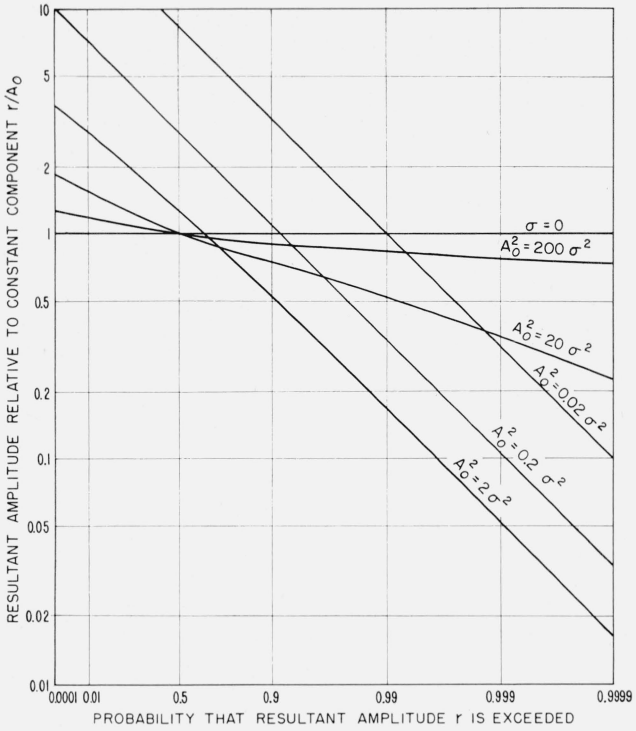

FIGURE 5.—*Probability that the total amplitude exceeds a given level, measured relative to the amplitude of the constant vector A_0, from [19].*

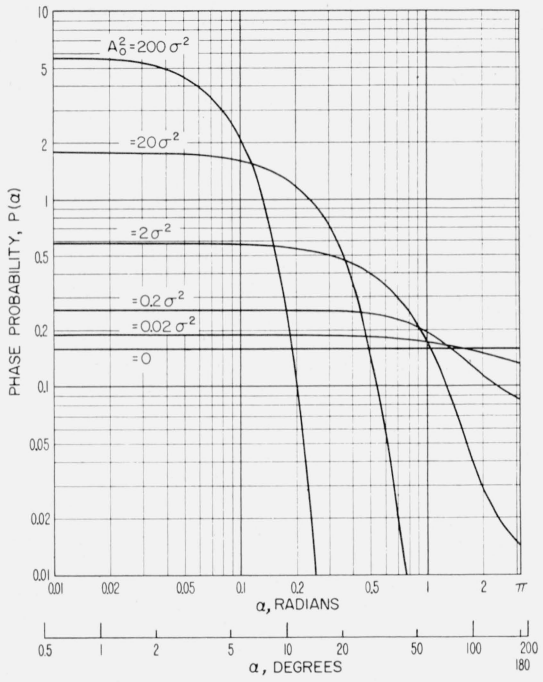

FIGURE 6.—*Distribution of phase variations about the reference voltage A_0 for line-of-sight propagation for various ratios of the steady signal to noise power.*

level distribution, but reduces the range of amplitude fading relative to A_0.

The distribution of phase is derived from eq (3.1.4) by integrating over all values of the amplitude A [20].

$$P(\alpha)d\alpha=\frac{d\alpha}{2\pi}e^{-A_0^2/2\sigma^2}\left\{1+\sqrt{\frac{\pi}{2}}\frac{A_0}{\sigma}\cos\alpha\, e^{A_0^2\cos^2\alpha/2\sigma^2}\times\left[1+\operatorname{erf}\left(\frac{A_0\cos\alpha}{\sqrt{2}\sigma}\right)\right]\right\} \quad (3.1.8)$$

This distribution is plotted in figure 6 and indicates that the phase is evenly distributed when the constant vector A_0 is very small compared with the rms multipath-scatter vector amplitude $\sqrt{2}\sigma$. When the constant vector is relatively large, Bremmer [20] proves that the phase is distributed about zero in a Gaussian manner,

$$\lim_{\sigma<<A_0} P(\alpha)\rightarrow\frac{A_0}{\sigma\sqrt{2\pi}}\exp-\left(\frac{A_0^2}{2\sigma^2}\right)\alpha^2, \quad (3.1.9)$$

Norton et al. [21] have also calculated the probability that the phase exceeds a given angle for various values of $A_0/\sqrt{2}\sigma$. The first and second moments of phase deviations have been evaluated numerically [22] using the result (3.1.8), and are reproduced in figure 7 as functions of $2\sigma^2/A_0^2$.

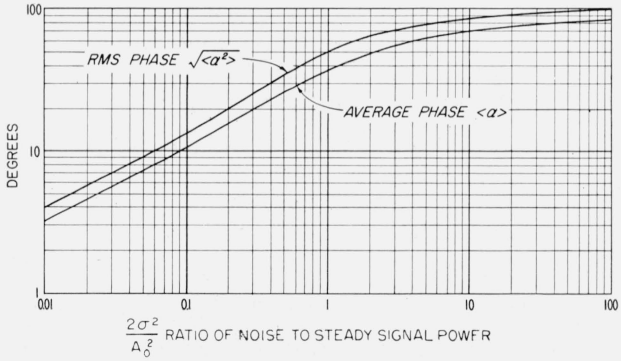

FIGURE 7.—*Average phase variation and root mean square phase variations about constant references voltage A_0 as functions of the amplitude ratio of signal-to-noise, from [22].*

Bremmer [20] has considered the probability distribution for time-displaced amplitudes (A_1, A_2) and phases (α_1, α_2) corresponding to figure 4. His development is based on special assumptions (see sec. 4.1.) for the time correlation between $x(t)$ and $y(t)$, but is quite interesting in that he establishes phase and phase-rate distributions for the same instant by manipulation of the probability density for time-displaced phases.

3.3. Electromagnetic Scattering by Irregularities

The stochastic dielectric constant (2.1.1) enters electromagnetic theory through the relation between the electric vector and displacement vector.

$$\vec{D}=\left[\epsilon_0+\Delta\epsilon(\vec{r},t)\right]\vec{E}. \tag{3.2.1}$$

When the magnetic field is eliminated from Maxwell's equations, the electric vector is found to satisfy [23],

$$\nabla^2\vec{E}-\frac{1}{c^2}\frac{\partial^2}{\partial t^2}[\epsilon\vec{E}]=-\vec{\nabla}\left[\frac{1}{\epsilon}\vec{E}\cdot\vec{\nabla}\epsilon\right]. \tag{3.2.2}$$

Time derivatives here operate principally on $\vec{E}$, since the field oscillates much more rapidly than the medium. The vector components of $\vec{E}$ are mixed in the right-hand term and give rise to depolarization effects. The magnitude of this term is small for line-of-sight microwave propagation and is usually omitted. (See, however, references [24] and [25].) With a harmonic time dependence ($k_f=\omega/c=2\pi/\lambda$), one finds

$$[\nabla^2+k_f^2(\epsilon_0+\Delta\epsilon)]\vec{E}=0, \tag{3.2.3}$$

which is the basic propagation equation.

It is not possible to solve (3.2.3) exactly, since $\Delta\epsilon(\vec{r},t)$ is an unknown (stochastic) function of position. The Born approximation is widely used to describe single scattering by such fluctuations. This is essentially a three-dimensional iterative solution of the wave equation, which gives the total field in terms of the unperturbed wave $\vec{E}_0(\vec{r})$ as

$$\vec{E}(\vec{R})=\vec{E}_0(\vec{R})-k_f^2\int_V d^3r G(\vec{R},\vec{r})\Delta\epsilon(\vec{r},t)\vec{E}_0(\vec{r})\sin\chi \tag{3.2.4}$$

where V is the volume of irregularities illuminated by both the transmitter and receiver, χ is the angle between $\vec{E}_0$ and the Poynting vector of the reradiated wave (see fig. 21) and is nearly 90 degrees for line-of-sight propagation. $G(\vec{R},\vec{r})$ is the free-space spherical Green's function connecting the scattering point $\vec{r}$ and receiver $\vec{R}$.

$$G(\vec{R},\vec{r})=\frac{e^{ik_f|\vec{R}-\vec{r}|}}{4\pi|\vec{R}-\vec{r}|} \tag{3.2.5}$$

The first term in (3.2.4) represents the transmitted wave and the integral expression is the scattered wave. The total field induces voltage components in the receiver, as shown in figure 4. The primary field E_0 sets the phase reference A_0. The integral term gives rise to the in- and out-of-phase random signal components $x(t)$ and $y(t)$, corresponding to the real and imaginary parts of the integral term in (3.2.4) respectively. The receiver measures the total voltage A and its phase α. It is inherent in the Born approximation that E_s must be small compared with the mean signal E_0, so that instantaneous fluctuations of the total amplitude and phase are (consistently) approximated by:

$$\delta A(t)\simeq x(t)=k_f^2\int_V d^3r\Delta\epsilon(\vec{r},t)\ \mathrm{Re}\ \{G(\vec{R},\vec{r})E_0(\vec{r})\}, \tag{3.2.6}$$

$$\alpha(t)\simeq\frac{y(t)}{A_0}=\frac{k_f^2}{E_0(\vec{R})}\int_V d^3r\Delta\epsilon(\vec{r},t)\ \mathrm{Im}\ \{G(\vec{R},\vec{r})E_0(\vec{r})\}. \tag{3.2.7}$$

The variances of phase and amplitude fluctuations thus depend upon six-fold integrals of the space correlation function (2.1.3)

It is common practice to use the geometrical optics approximation to describe line-of-sight propagation. This is equivalent to a one-dimensional (WKB) solution of the wave eq (3.2.3), which recognizes only the random speeding-up and slowing-down of the wave as it propagates along the ray path (s). The phase of the vector voltage diagram in figure 4 is given directly by this method,

$$\alpha=\frac{\pi}{\lambda}\int_0^L ds\Delta\epsilon(s,t), \tag{3.2.8}$$

and is to be computed along the nominal (rectilinear) ray path s. This expression is always a good approximation to the volume integral (3.2.7), and it is generally used to study phase variations because of its simplicity. Geometrical optics also predicts amplitude variations of the received signal. These are due physically to bunching and diverging of the energy-bearing rays by random refractive bending;

$$\frac{\delta A}{A_0}=\frac{\lambda}{2\pi}\int_0^L ds\left[\frac{\partial^2\alpha}{\partial x^2}+\frac{\partial^2\alpha}{\partial y^2}\right] \tag{3.2.9}$$

where α is given by expression (3.2.8). This expression is usually not a good approximation to the more precise wave theory result (3.2.6).

The geometrical optics approximation is a special case of the single scattering wave theory of eq (3.2.4) [4, 5, 26]. To understand this correspondence, note that the scale length of the irregularities l_0 is ordinarily much larger than the wavelength of the radiation. The blobs act like very shallow lenses and project almost all of the scattered radiation in a cone of angular opening λ/l_0 about the line-of-sight. The effective scattering volume over a path length L, therefore, has a maximum width $L\lambda/l_0$ as shown in figure 8. If this width is much less than the average blob size, the scattering volume consists of cylindrical plugs "cored" from successive blobs as in figure 8a. The propagation is then substantially one dimensional

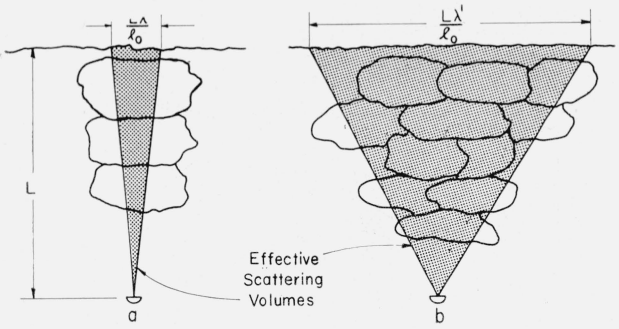

FIGURE 8. *Pictorial representation of the effective scatter volume for line-of-sight radio star problem: (a) Fresnel scattering, and (b) Fraunhofer scattering.*

and random variation of the phase speed of the wave is the measured effect. This corresponds to Fresnel scattering and is correctly treated by geometrical or ray optics. The opposite extreme occurs when $L\lambda/\pi l_0 > > l_0$; the receiver sees many whole blobs as in figure 8b. The problem is then necessarily three dimensional and requires the wave solution (3.2.4), corresponding to Fraunhofer scattering. The scattering parameter

$$\gamma = \frac{L\lambda}{l_0^2} \tag{3.2.10}$$

is evidently the important variable in these discriminations. One finds that the wave theory expressions (3.2.6) and (3.2.7) reduce exactly to the geometrical optical results (3.2.9) and (3.2.8) if γ is less than unity. If γ is greater than (or near) unity, however, one must use the full-wave theory to compute amplitude scintillations.

The single-scattering approximation (3.2.4) breaks down at large distances L and/or high frequencies, since the convergence of the Born series is related to the smallness of the mean square phase expression [5],

$$<\alpha^2> \cong \pi^2 <\Delta\epsilon^2> \frac{Ll_0}{\lambda^2}. \tag{3.2.11}$$

As the wave progresses deeper into the turbulence, scattering out of the main beam gradually dissipates the primary signal A_0 in figure 4 and one is left only with the correspondingly increased random field E_s. The method of Rytov [27] has been used to describe this "phase creep" zone, where the amplitude and phase fluctuations are not small.

$$\vec{E}(\vec{R}) = \vec{E}_0(\vec{R}) \exp - \left[\frac{k_f^2 \rightarrow}{\vec{E}_0(\vec{R})} \cdot \int d^3 r G(\vec{R},\vec{r}) \Delta\epsilon(\vec{r},t) \vec{E}_0(\vec{r}) \right] \tag{3.2.12}$$

This expression reduces to (3.2.4) in the limit of small signal variations, but it is not clear how this method accounts for multiple scatterings. It is significant that the integral term in the exponent of Rytov's expression is identical to the first Born term in eq (3.2.4). Difficult propagation calculations of the real and imaginary parts of this integral term computed for single scattering theory can thus be used in calculations based on (3.2.12), once the appropriate signal-statistical description is established.

Feinstein [28] used the Kirchhoff-Huygens approximation to study propagation of scalar waves through a succession of uncorrelated random slabs. His use of the second order phase approximation is equivalent to tracing the phase front along various ray paths, or neglecting diffraction over the slab thickness. The result can be expressed as a power series in $<\Delta\epsilon^2>$, the first term of which is the geometrical-optics approximation.

3.4. Propagation Calculations Based on Geometrical Optics

The foregoing discussion presented general expressions for the phase and amplitude scintillations of waves which are propagated through random media. To compare theory and experiment, it is necessary to combine these propagation expressions with the descriptions of turbulent media given in part II. The results depend both on the propagation geometry and the model chosen to represent the irregularities.

The calculation of phase variations is usually based on the geometrical optics approximation. The variance of phase fluctuations $<\alpha^2>$ about the constant reference vector A_0 can be computed by simply squaring and averaging the integral expression (3.2.8). Using any of the correlation models described in section 2.2 gives the following simple result,

$$<\alpha^2> = q\pi^2 <\Delta\epsilon^2> \frac{Ll_0}{\lambda^2}, \tag{3.3.1}$$

where L is the line-of-sight path length and λ the wavelength of the radiation employed. q is a constant of order unity which has been evaluated for each of the four correlation models. References to such detailed calculations are summarized in table 2, together with references to other phase and angle-of-arrival quantities. The reader should consult these references for specific results.

The wavelength dependence of expression (3. 3. 1) has been confirmed experimentally by simultaneous measurements [33, 34] of phase shifts on three frequencies, 100, 1,000, and 10,000 Mc, on line-of-sight paths to mountain tops. The path length (L) dependence is difficult to check experimentally, since paths of different lengths are apt to go through regions of the troposphere which do not have the same level of turbulent activity. Attempts to correlate phase variations with airborne and ground-based refractometer measurements of $<\Delta\epsilon^2>$ and l_0 in the propagation paths have been moderately successful [3, 30].

Such results are conveniently summarized with the

TABLE 2. *References for line-of-sight calculations of phase and amplitude fluctuations using geometrical optics for four space correlation models of the irregularities*

Calculated quantity \ Space correlation model	Bessel $\rho K_1(\rho)$	Exponential $e^{-\rho}$	Gaussian $e^{-\rho^2}$	Cauchy $[1+\rho^2]^{-2}$
Mean square phase	30	29, 30	29, 30	29, 30
Finite path corrections to $<\alpha^2>$	30	30	30	30
Aperature smoothing corrections to $<\alpha^2>$	31	31	31	----
Finite data sample corrections to $<\alpha^2>$	----	----	----	----
Parallel path space correlation	----	29	29	29
Rotated path space correlation	30	29	29	29
Time correlation of phase	30	29, 30	29, 30	29, 30
Power spectrum of phase	30	29, 30	29, 30	29, 30
Phase fading rate	30	Diverges	32	32
Number of phase maxima	Diverges	Diverges	----	----
Mean square angle-of-arrival	----	Diverges	29	29
Time correlation of angle-of-arrival	----	29	29	29
Spectrum of angle-of-arrival	----	29	29	29
Mean square amplitude variance	Diverges	Diverges	----	----

spectrum method, suggested in section 2.3, where a model choice is delayed until after the *propagation* calculations have been performed. In terms of the blob-size spectrum $S(k)$, the mean square phase fluctuation becomes [4]:

$$<\alpha^2>=\frac{\pi L}{2\lambda^2}\int_0^\infty dk k S(k), \qquad (3.3.2)$$

which exhibits directly the dependence of the measured ($<\alpha^2>$) on the controlled variables L and λ. The spectrum method is particularly advantageous when computing corrections to this expression due to aperature smoothing, finite data sample lengths (T) and finite propagation path lengths (L). These effects can be analyzed exactly within the framework of geometrical optics, and produce appropriate factors in the wavenumber integration which filter the spectrum $S(k)$ preferentially. Analyzing the individual effects separately and multiplying them serially one finds [4].

$$<\alpha^2>=\frac{\pi L}{2\lambda^2}\int_0^\infty dk k S(k)\left[\frac{2J_1(ka)}{ka}\right]^2 \times\left[\frac{2}{\pi}\left\{Si(kL)-\frac{1-\cos(kL)}{kL}\right\}\right] \times\left[1-\frac{2}{kUT}\int_0^{kUT}dz J_0(z)+2\frac{J_1(kUT)}{kUT}\right]. \qquad (3.3.3)$$

This composite spectrum filtering is illustrated in figure 9. The first factor accounts for the masking of small blob (large wavenumber) contributions to $<\alpha^2>$ due to smoothing by a receiving aerial of

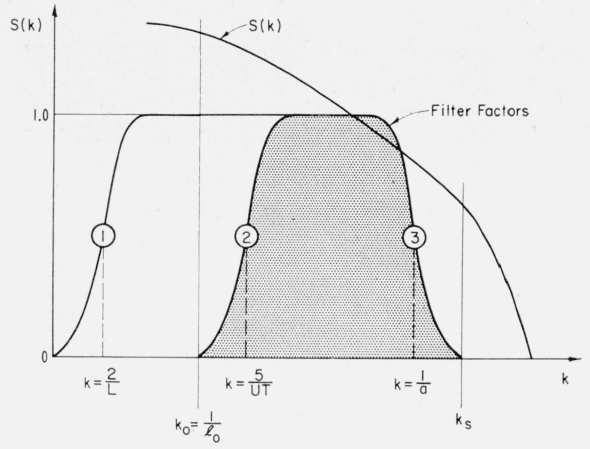

FIGURE 9. *Typical spectrum showing preferential filtering factors: (1) finite path length, (2) finite data sample length, and (3) aperture smoothing corrections.*

radius a. The second factor describes finite path length correlations, and indicates that blobs larger than the total path length L cannot contribute effectively to signal fluctuations. The last factor describes the effect of a finite data sample length T in suppressing very low-frequency scintillations, assuming that they are due only to a convective speed U. This predicts that the rms phase variation should increase with sample length T, which is observed experimentally [3]; although nonstationary trends could give the same result. References to explicit calculations of the individual effects for various spectral models (i.e., correlation functions) are given in table 2.

The space correlation between phase variations measured on adjacent propagation paths has been calculated for a variety of turbulence models (see table 2) for both the rotated line-of-sight and parallel path configurations indicated in figure 10.

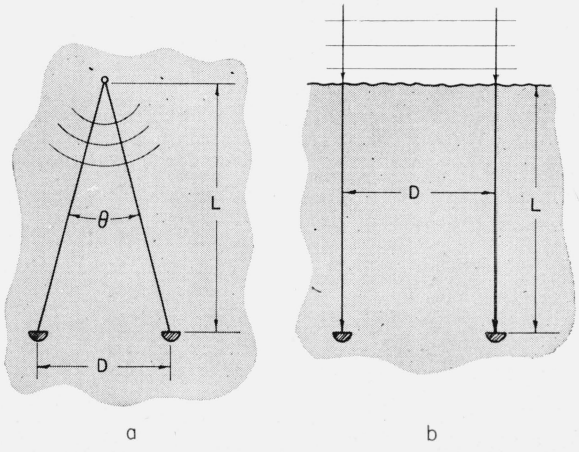

FIGURE 10. *Geometry for space correlation of phase experiments: (a) Rotated paths with common transmitter and (b) parallel rays from source of infinity.*

The spectrum method summarizes these results in succinct form [4].
Parallel rays:

$$<\alpha(x)\alpha(x+D)>=\frac{\pi L}{2\lambda^2}\int_0^\infty dkkS(k)J_0(kD), \quad (3.3.4)$$

Rotated rays:

$$<\alpha(\phi)\alpha(\phi+\theta)>=\frac{\pi L}{2\lambda^2}\int_0^\infty dkkS(k)\,\frac{1}{kL\theta}\int_0^{kL\theta} duJ_0(u). \quad (3.3.5)$$

These filter factors essentially eliminate the contribution of small blobs (large wavenumbers), which are not large enough to affect both paths simultaneously.

It is found that the Bessel model gives good agreement with spaced receiver experiments [33,30] for small baseline distances. At very large separations, however, the experimental correlation falls more slowly than the theory predicts. This is tentatively ascribed to lack of spatial homogeneity and/or temporal stationarity. Since the correlation at great distances is due to the joint influence of very large blobs on the two propagation paths, the phase correlation should depend on the large R behavior of $C(R)$, which is not tied to physical theories, as noted in section 2.4.

The random variation of single path phase records with time is due to the action of drifting convection and turbulent self motion. The space-time correlation of dielectric fluctuations (2.5.3) permits one to calculate the time correlation of phase records quite generally for an arbitrary spectrum. If the convective wind blows normal to the propagation path [4],

$$<\alpha(t)\alpha(t+\tau)>$$

$$=\frac{\pi L}{2\lambda^2}\int_0^\infty dkkS(k)J_0[kU\tau]\eta[k,\tau]. \quad (3.3.6)$$

The effect of self-motion is usually discarded (i.e., $\eta=1$), since the turbulent speed (V_0) is much less than the drift speed U.

The experimental data on phase scintillations is usually expressed in terms of frequency spectra of the phase records. For drift motion alone [5],

$$W(f)=\frac{\pi L}{2\lambda^2}\int_{\frac{2\pi f}{U}}^\infty \frac{dkkS(k)}{[k^2U^2-(2\pi f)^2]^{1/2}}. \quad (3.3.7)$$

The mixing-in-gradient model (2.4.6) predicts that the frequency spectrum $W(f)$ should vary as f^{-4}, while the Obukhov model (2.4.4) predicts an $f^{-2.7}$ variation. The most recent data [3] indicates a frequency variation of $f^{-2.8}$ from 1 cycle per hour to 10 cps for very low-level paths. This data argues strongly for the Obukhov Mixing Theory, unless self-motion effects play a dominant role.

The average number of mean (zero) crossings and maxima can be expressed in terms of ratios of moments of the frequency spectrum $W(f)$, which in turn can be related to moments of the turbulent spectrum $S(k)$[4]. Filter factors at the high-wavenumber end, such as that provided by aperture smoothing, are especially important if such results are to be compared with experimental data.

Tracking devices which measure bearing angles ordinarily measure the normal to the instantaneous phase front by interferometric means. Angle-of-arrival errors are thus related to the space coherence (correlation) of phase scintillations along this phase front. The mean square angle of arrival is given by [4]

$$<\delta\theta^2>=\frac{L}{16\pi}\int_0^\infty dkk^3S(k), \quad (3.3.8)$$

and has been evaluated explicitly in the references of table 2. The autocorrelation of $\delta\theta(t)$ and the corresponding frequency spectrum have also been discussed in general [4] and specific terms [29].

Amplitude fluctuations have not received as much attention as phase (see however, ref [36] and [37]) since $\delta A/A_0$ must be small compared with $(\alpha)_{\text{rms}}$ for the geometrical optics expression (3.2.9) to be valid. In terms of the spectrum, the percentile amplitude fluctuation is given by

$$\left\langle\left|\frac{\delta A}{A_0}\right|^2\right\rangle\simeq L^3\int_0^\infty dkk^5S(k), \quad (3.3.9)$$

which depends critically on the behavior of the correlation model near the origin (i. e., $k=\infty$). Only the Gaussian and Cauchy correlation models predict finite results, viz,

$$\left\langle\left|\frac{\delta A}{A_0}\right|^2\right\rangle=g\langle\Delta\epsilon^2\rangle\,\frac{L^3}{l_0^3}, \quad (3.3.10)$$

where g is a constant of order unity. This distance variation and absence of a frequency dependence does not agree with most experiments [33, 38], so one must seek a more satisfactory solution in the wave theories.

3.5. Propagation Calculations Based on Wave Theory

When the scattering process is necessarily three-dimensional in the sense of figure 8, one must use the Born expressions (3.2.6) and (3.2.7) for line-of-sight amplitude and phase. The variance of phase and amplitude depend upon six-fold integrals of the space correlation function (2.1.3). Such calculations have been performed primarily with the Gaussian function, which has important analytical-simplification properties, although even then one must exploit approximations.

The spectrum method has simplified the evaluation of these wave theory expressions enormously. Using the method described previously [4], one can establish the following general expressions for the radio-star problem:

$$\left\langle \alpha^2 \right\rangle = \frac{\pi L}{2\lambda^2}\int_0^\infty dk k S(k)\left[1-\Phi\left(\frac{k^2 L\lambda}{2\pi}\right)\right],$$

$$\left\langle \left|\frac{\delta A}{A_0}\right|^2 \right\rangle = \frac{\pi L}{2\lambda^2}\int_0^\infty dk k S(k)\Phi\left(\frac{k^2 L\lambda}{2\pi}\right),$$

$$\left\langle \left|\alpha \frac{\delta A}{A_0}\right| \right\rangle = \frac{\pi L}{2\lambda^2}\int_0^\infty dk k S(k)\Psi\left(\frac{k^2 L\lambda}{2\pi}\right), \quad (3.4.1)$$

where the fundamental scattering filter functions are defined by

$$\Phi(x) = \frac{x^2}{2(1+x^2)} + 0\left(\frac{1}{kL}\right), \quad (3.4.2)$$

$$\Psi(x) = \frac{x}{2(1+x^2)} + 0\left(\frac{1}{kL}\right). \quad (3.4.3)$$

The corresponding filter factors in the spectral integrals of (3.4.1) are plotted together in figure 11.

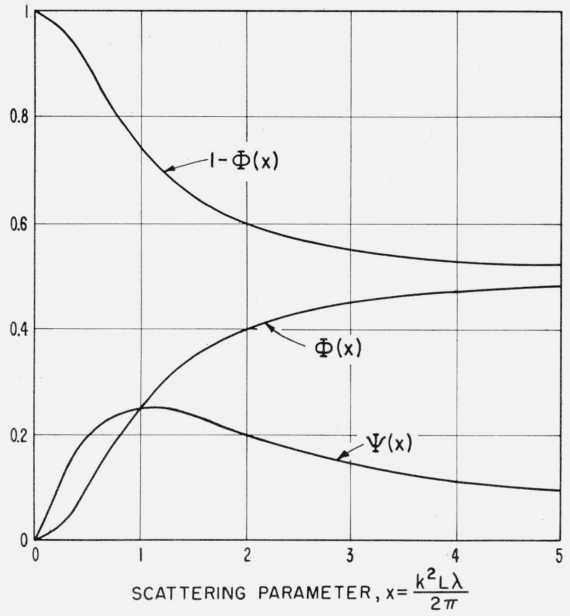

FIGURE 11. *Fundamental scattering filter factors for wave theory treatments of line-of-sight propagation.*

These functions depend upon the scattering parameter $\gamma = k^2 L\lambda$ for each blob-size group in the distribution described by $S(k)$. Those blobs in $S(k)$ which scatter in the Fraunhofer zone ($\gamma \gg 1$) produce equal phase and amplitude variations, each one-half as great as the ray theory result (3.3.2). The Fresnel regime ($\gamma \ll 1$) gives the geometrical optics phase result (3.3.2) directly. Using the small argument behavior $\Phi(x) \simeq \frac{x^2}{2}$, the geometrical optics result for amplitude fluctuations (3.3.9) is regained.

Explicit expressions for the phase and amplitude correlations can be established by introducing a particular spectrum model from table 1 into (3.4.1) and performing the single remaining wavenumber integration. Barrows [35] has evaluated these integrals for the Exponential, Gaussian, and Bessel models, and finds

$$\langle \alpha^2 \rangle = \frac{2\pi^2 \langle \Delta\epsilon^2 \rangle L l_0}{\lambda^2} F\left(\frac{L\lambda}{2\pi l_0^2}\right)$$

$$\left\langle \left|\frac{\delta A}{A_0}\right|^2 \right\rangle = \frac{2\pi^2 \langle \Delta\epsilon^2 \rangle L l_0}{\lambda^2}\left[1 - F\left(\frac{L\lambda}{2\pi l_0^2}\right)\right]$$

$$\left\langle \alpha \frac{\delta A}{A_0} \right\rangle = \frac{2\pi^2 \langle \Delta\epsilon^2 \rangle L l_0}{\lambda^2} G\left(\frac{L\lambda}{2\pi l_0^2}\right) \quad (3.4.4)$$

where the scattering parameter-dependent functions have approximately the same form as the filtering functions $\Phi(x)$ and $\Phi(x)$. The results obtained in this way are substantially the same as those obtained by Fannin [42], Mintzer [6], Obukhov [39], and Chernov [40] by the more laborious direct calculation of six-fold volume integrals. Since their results differ in details of propagation geometry, space correlation models, and scattering theory, we have constructed table 3 to summarize the essential assumptions and results of each paper.

The derivation of expressions (3.4.1) given in reference [4] does not lend itself to calculating space and time correlation effects. A new method was devised which combines the integral expressions (3.2.6) and (3.2.7) with the original representation

TABLE 3. *Explicit calculations of phase and amplitude fluctuation quantities using three dimensional wave theory*

Author	Reference	Scattering theory	Propagation model	Space correlation model	Phase variation	Amplitude variance	Phase-amplitude correlation	Space correlation	Time correlation	Others
Obukhov	39	Rytov	Radio star	Gauss	✓	✓				
Chernov	40	do	do	do	✓	✓	✓	✓		
Tatarski	41		do	Exp		✓				
Mintzer	6	Born	Relay link	Gauss		✓			✓	✓
Fannin	42	do	do	do	✓	✓		✓	✓	
Ellison	26	do	Radio star	do		✓		✓		
Wheelon	23	do	do	do	✓	✓		✓		
Barrows	35	do	do	Bessel Gauss	✓	✓	✓			
Wheelon	5	do	do	General	✓	✓				

(2.3.1) of the space correlation function, rather than the specialized form of eq (2.3.2). For example,

$$\langle\alpha^2\rangle = k_f^4 \int_V d^3r \,\mathrm{Im}[G(\vec{R},\vec{r})\,E_0(\vec{r})] \int_V d^3r' \,\mathrm{Im}[G(\vec{R},\vec{r}')\,E_0(\vec{r}')]$$

$$\times \frac{1}{8\pi^3} \int d^3k S(k) \exp i\vec{k}\cdot(\vec{r}-\vec{r}')$$

$$= \frac{k_f^4}{8\pi^3} \int d^3k S(k) \left| \int_V d^3r e^{i\vec{k}\cdot\vec{r}} \,\mathrm{Im}\,[G(\vec{R},\vec{r})\,E_0(\vec{r})] \right|^2 \tag{3.4.5}$$

Barrows [35] has found that the volume integral can be evaluated rigorously for either the radio star or relay link problem. In principle one can include the influence of ground reflections indicated in figure 12, by simply redefining the Green's function $G(R,r)$ and incident field $E_0(r)$ in eq (3.4.5) to satisfy the boundary conditions at the earth's surface. This can be accomplished analytically for a perfectly conducting earth by simply adding image sources and image scattering blobs to represent the ground-bounce paths.

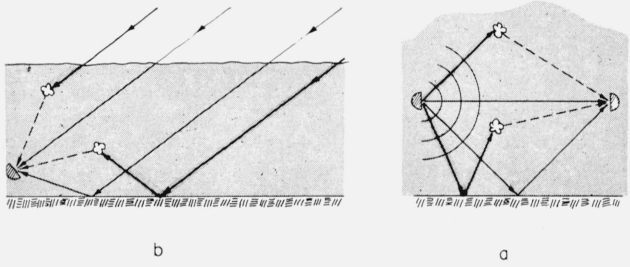

FIGURE 12. *Typical ray paths for line-of-sight propagation including ground reflected effects: (a) Relay link & (b) radio star problems.*

The new representation (3.4.5) is well adapted to describing time autocorrelations of the phase. Using the space-time correlation spectral representation (2.5.2), we find

$$\langle\alpha(t)\alpha(t+\tau)\rangle = \frac{k_f^4}{8\pi^3} \int d^3k S(k)\eta(k,\tau) e^{-i\vec{k}\cdot\vec{U}\tau}$$

$$\times \left| \int_V d^3r e^{i\vec{k}\cdot\vec{r}} \,\mathrm{Im}\,[G(\vec{R},\vec{r})\,E_0(\vec{r})] \right|^2 \tag{3.4.6}$$

which uses precisely the same geometrical propagation integrals required for the phase variance calculation in (3.4.5). Space correlations follow directly if one replaces the drift displacement $\vec{U}\tau$ with the receiver separation $\vec{D}$, providing the appropriate displaced coordinate system indicated by figure 13 is employed. If the wavenumber integration is performed in polar coordinates, it is found that the geometrical integrals do not depend on the (k) azimuth angle, and therefore,

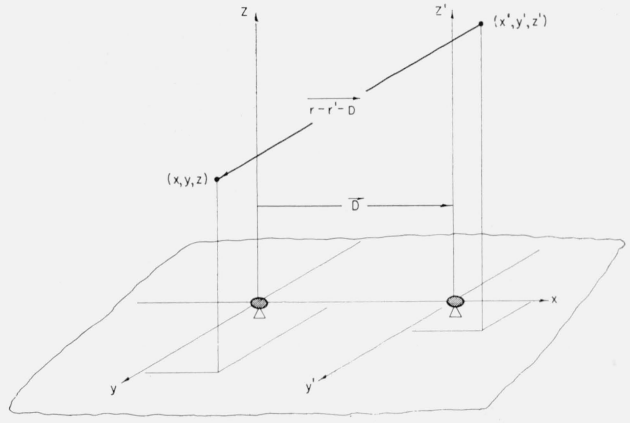

FIGURE 13. *Coordinates for calculation of phase correlation between adjacent receivers.*

$$\langle\alpha(x)\alpha(x+D)\rangle = \frac{k_f^4}{16\pi^2} \int_0^\infty dk k^2 S(k) \int_0^\pi d\theta \sin\theta J_0(kD\sin\theta)$$

$$\times \left| \int_V d^3r e^{i\vec{k}\cdot\vec{r}} \,\mathrm{Im}\,[G(\vec{R},\vec{r})\,E_0(\vec{r})] \right|^2. \tag{3.4.7}$$

The effect of aperture smoothing with a circular parabolic dish of radius a can be evaluated by the same integration technique used with the less accurate geometrical optics solution [4, 31].

$$\langle\alpha_T^2\rangle = \left\langle \left| \frac{1}{A} \iint_A d\sigma\alpha(\sigma) \right|^2 \right\rangle$$

$$= \frac{k_f^4}{16\pi^2} \int_0^\infty dk k^2 S(k) \int_0^\pi d\theta \sin\theta \left[\frac{2J_1(ka\sin\theta)}{ka\sin\theta} \right]^2$$

$$\times \left| \int_V d^3r e^{i\vec{k}\cdot\vec{r}} \,\mathrm{Im}\,[G(\vec{R},\vec{r})\,E_0(\vec{r})] \right|^2 \tag{3.4.8}$$

Even the difficult question of polarization dependence can be discussed conveniently in this framework, if a tensor Green's function is used in the Born approximation [24, 25]. In this way one can build up theoretical estimates of considerable interest to measurement programs. The method keeps the geometrical and turbulence problems separated until the last possible step, so as to allow each to develop as fully as possible.

3.6. Physical Interpretation of Scattering

It is valuable to pause briefly to re-examine the mathematical expressions (3.2.4) introduced by the Born approximation. Figure 14a indicates a typical singly-scattered ray trajectory for the radio-star problem. The scattered ray path concept may be identified with terms in the integrand of (3.2.4). The incident plane wave $\vec{E}_0(\vec{r})$ propagates rectilinearly to the scattering volume element d^3r. The dielectric fluctuations $\Delta\epsilon(\vec{r},t)$ scatters a small fraction

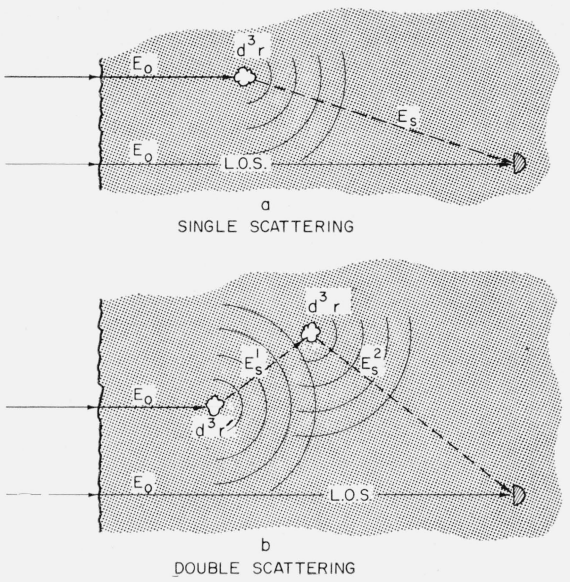

FIGURE 14. *Ray paths for single and double scattering of plane wave by a semi-infinite region.*

of the wave $\vec{E}_0(\vec{r})$ in all directions. (This reradiation is strongly concentrated in the forward direction, since the refractive variations act like very weak, overlapping lenses with radii of curvature l_0 much larger than the radiation wave length λ). A portion of the scattered energy is propogated along the line connecting the receiver $\vec{R}$ and scatterer $\vec{r}$. The propagation of this component is described by the Green's function (3.2.5), which characterizes the spherical expansion of the (unit) scattered wave. The total scattered field is simply the summation of all such multipath contributions, as given by the integration (3.2.4). These scattered waves are out of phase with respect to the primary signal $\vec{E}_0$ propagated along the line-of-sight, in virtue of their longer path lengths. Random fluctuations of the strength of these scattered components (i.e., $\Delta\epsilon$) give rise to the characteristic fading suggested by figure 4.

The typical ray path for double scattering processes indicated in figure 14b can be compared with the second Born approximation

$$E(\vec{R}) = E_0(\vec{R}) - k_f^2 \int_V d^3r G(\vec{R},\vec{r}) \Delta\epsilon(\vec{r},t) E_0(\vec{r}) + k_f^4 \int_V d^3r \int_V d^3r' G(\vec{R},\vec{r}) \Delta\epsilon(\vec{r},t) G(\vec{r},\vec{r}') \Delta\epsilon(\vec{r}',t) E_0(\vec{r}') \tag{3.5.1}$$

The double integral term has the following meaning: an incident wave $\vec{E}_0(\vec{r}')$ falling on the first scattering element d^3r' is scattered by $\Delta\epsilon(\vec{r}',t)$, and reradiated to $\vec{r}$ by $G(\vec{r},\vec{r}')$. The second element $\Delta\epsilon(\vec{r},t)$ scatters the wave again and reradiates the result to the receiver via $G(\vec{R},\vec{r})$. The double integration simply sums the contributions over all possible pairs of scattering elements.

This tracing of rays between scattering events is similar to Feynman's diagramatic technique for describing the space-time history of particles in Quantum Electrodynamics [43]. In treating the dielectric fluctuations $\Delta\epsilon$ as a sequence of scattering events, however, one must give up the concept of a continuously refracting medium. Phase fluctuations are no longer regarded as the result of random changes in the velocity of propagation along the line-of-sight path. Rather, phase instability is looked upon as the random composition of many multipath components with the primary signal (see ref [44]).

Our description has been something less than accurate thus far in that expansions like (3.5.1) imply more power at the observation point $\vec{R}$ than would have appeared in the absence of refractive fluctuations $|E_0|^2$. We have evidently overlooked scattering out of the primary beam on the line-of-sight ray path to the receiver. A scattering event robs the beam of some energy at each point along this path. Such losses are just compensated by energy which is projected back into the receiver by off-axis blobs. Inspection of figure 15 shows that for each point to which the line point scatters energy out of the beam, there is a corresponding point on the wave normal which projects an equal amount of energy back into the receiver at the same angle. If the receiver is isotropic, the two effects just cancel.

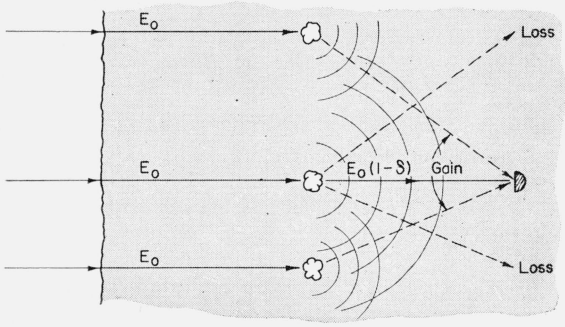

FIGURE 15. *Singly-scattered ray paths for radio star problem indicating power balance between scattering losses out of the beam and projection of energy into the receiver by off-axis blobs.*

Energy can re-enter the primary ray only by a double scattering process, which changes its direction back to the original line-of-sight. This means that the power balance must be maintained at each level of iteration, and is related to the unitary relationships which must hold between the various terms in the Born series. It is important to observe that such conservation cannot be demanded of the fluctuating field strength, but only of the averaged power.

4. Scatter Propagation

The transmission of telephonic and even television signals well beyond the optical horizon at UHF frequencies is such an important component of world-wide communications today that it requires no historical introduction. Suffice it to say that weak but dependable communication signals are received out to distances of 1,000 km if sufficient transmitter power and receiver sensitivity are employed. The signal envelope is observed to fade in an irregular manner. This suggested that the propagation might be due to radiowave scattering by the refractive irregularities (turbulence) which were known to exist in the troposphere. The mathematical theory of this scattering was developed by Pekeris [45] and Booker and Gordon [46], using the single scattering approximation.

The refractive scattering explanation of microwave propagation beyond the horizon is illustrated by figure 16. Turbulent blobs in the common volume of the receiver and transmitter are imagined to scatter minute fractions of the line-of-sight fields into the receiver. The case of omnidirectional aerials is shown in figure 16a, and indicates that the common volume is defined by the tangent planes to the transmitter and receiver. The incoherent addition of signal contributions throughout this volume gives rise to random orthogonal voltage components in the receiver, as suggested by the drawing. The narrow-beam case, shown in figure 16b, indicates that the corresponding scattering volume is controlled by the antenna patterns.

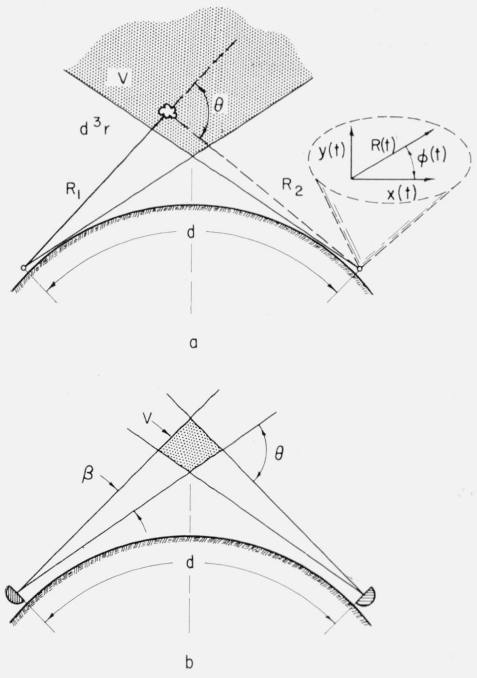

FIGURE 16. *Geometry for scatter propagation beyond the horizon: (a) Broad beam aerials, and (b) narrow beam aerials.*

A substantial amount of reliable experimental data was first published in 1955 [47]. The overall experimental situation at that time was ably summarized by Bullington's review paper [48]. Additional results have been published sporadically in succeeding years, and it is somewhat difficult to establish the precise state of affairs at this time. An up-to-date summary of theoretical research on the subject in the United States was presented to URSI in 1957 by Staras and the author [49]. The following section extends that report by describing a considerable amount of unpublished work. We also attempt to correlate the theoretical predictions with experimental results where possible.

4.1. Signal Statistics and Vector Voltage Diagram

The electromagnetic field received beyond the horizon via the scatter mode induces a complex voltage

$$x(t)+iy(t)=R(t)\ e^{i\phi(t)} \tag{4.1.1}$$

in the receiver, as shown in figure 16. The orthogonal signal components x and y result from the in and out-of-phase incoherent addition of waves scattered from many independent blobs in the common volume. Application of the Central Limit Theorem to this scattering process by many blobs ensures that $x(t)$ and $y(t)$ are distributed in a Gaussian manner. The components change randomly with time because of the changing phase relationships of the scattering contributions from randomly moving blobs. The processes $x(t)$ and $y(t)$ are probably stationary over brief observation periods, but do exhibit diurnal and seasonal variations which are quite predictable.

The probability distribution for amplitude $R(t)$ and phase $\phi(t)$ at a fixed time t can be computed directly from the Gaussian distribution for $x(t)$ and $y(t)$ suggested above. It is usually assumed that both these components have equal variances σ^2 in the far field scattering range of beyond-the-horizon propagation.

$$P(x,y)dxdy=\frac{dxdy}{2\pi\sigma^2\sqrt{1-\rho^2}}\exp-\left\{\frac{x^2+y^2-2\rho xy}{2\sigma^2(1-\rho^2)}\right\},$$

where

$$\langle x^2\rangle=\langle y^2\rangle=\sigma^2$$

$$\langle xy\rangle=\sigma^2\rho.$$

Transformation to the polar coordinates of (4.1.1) yields the joint amplitude-phase distribution.

$$P(R,\phi)\,RdRd\phi=\frac{RdRd\phi}{2\pi\sigma^2\sqrt{1-\rho^2}}\exp-\left\{\frac{R^2[1-\rho\,\sin^2\phi]}{2\sigma^2(1-\rho^2)}\right\} \tag{4.1.2}$$

Previous discussions of random signals have taken the cross-correlation (ρ) between the in and out-of-

phase components to be zero. This is justified for electrical shot noise which is a randomly phase-modulated signal. It is not justified for scatter signals, which are essentially amplitude-modulated. This cross correlation has been computed explicitly for line-of-sight propagation geometries [40], and is definitely not zero in that case. Although a similar calculation needs to be performed for scatter propagation geometries, it is quite possible that ρ has a finite value.

The distribution of signal amplitudes is established by integrating (4.1.2) over all values of the phase, ($-\pi$ to π).

$$P[R]RdR=\frac{dRR}{\sigma^2\sqrt{1-\rho^2}}\,I_0\left[\frac{R^2}{2\sigma^2}\,\frac{\rho}{1-\rho^2}\right]\exp-\left[\frac{R^2}{2\sigma^2(1-\rho^2)}\right] \tag{4.1.3}$$

If the cross correlation ρ were zero, this would reduce to the Rayleigh distribution for R [50, 51]. The root mean square amplitude is independent of ρ,

$$R_{rms}=\sqrt{\langle R^2\rangle}=\sigma\sqrt{2} \tag{4.1.4}$$

and forms a convenient amplitude reference.

The probability that the amplitude exceeds a given level r is obtained by integrating (4.1.3) from r to infinity, and is plotted in figure 17. The theoretical curves for different ρ are plotted on Rayleigh paper, so as to exhibit departures from the straight line plot of a simple Rayleigh distribution ($\rho=0$). This curve indicates that finite values for the cross correlation enhance large values of R relative to those of the Rayleigh distribution. The probability of observing very small signal values is correspondingly smaller than for the Rayleigh case. It is quite significant that this very departure has been observed experimentally on many scatter links [47, 52]. It should also be noted, however, that a signal level trend superimposed on the random amplitude process would produce the same general behavior for finite data samples.

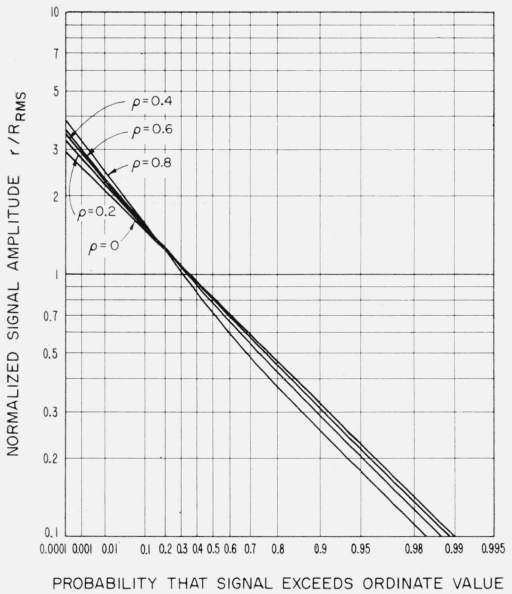

FIGURE 17. *Probability that instantaneous signal amplitude exceeds a given level measured in terms of the RMS signal level for various cross correlations* ρ.

The possibility of a steady signal being admixed with the random scatter signal cannot be ignored, especially on short paths where the ground wave or reflecting layers may be important. The corresponding statistical problem of a constant vector plus a random process was summarized in section 3.1. It is apparent that the entire signal level distribution is raised by such an addition, which offers a third possible explanation for the non-Rayleigh character of the signal level distributions.

The average signal level can be computed from (4.1.3).

$$\langle R\rangle=\sigma\,\frac{\sqrt{\pi}}{2}\left[\sqrt{1+\rho}\,\frac{2}{\pi}\,E\left(\frac{\sqrt{2\rho}}{1+\rho}\right)\right], \tag{4.1.5}$$

where $E(x)$ is the complete elliptic function of the second kind. The correlation-dependent factor in square brackets varies by only ten percent over the entire range of ρ, so the Rayleigh form is an adequate expression.

The distribution of signal phases can be established by averaging (4.1.2) over all possible amplitudes.

$$P[\phi]d\phi=\frac{d\phi}{2\pi}\,\frac{\sqrt{1-\rho^2}}{1-\rho\sin 2\phi} \tag{4.1.6}$$

This is plotted in figure 18 for $0<\phi<\pi$ (since it is symmetric about the origin) and various ρ, indicating the departure from a uniform phase distribution which is usually associated with a Rayleigh distribution of amplitudes.

The foregoing description applies to the signal fluctuations observed during an interval ranging from several minutes to several hours. A substantial amount of experimental data is presented in terms of distributions of hourly medians, which are found to be "log-normally" distributed [53]. McCrossen [54] used this experimental result to suggest a phenomenological theory of nonstationary signal distributions for all time spans. The essential idea is to treat the signal variance in eq (4.1.3) as a long-term random variable. It is assumed that σ is sufficiently constant over intervals required for the averaging of short-term fluctuations. The quantity which is observed to be log-normally distributed is the hourly median of received power,

$$Z=P_{0.5}=\sigma^2\log 4=\langle R^2\rangle\log 2, \tag{4.1.7}$$

where ρ is taken to be zero for convenience. The distribution for Z is thus

$$P(Z)dZ=\frac{1}{\sqrt{2\pi}\zeta}\,\frac{dZ}{Z-Z_0}\exp-\left[\frac{[\log(Z-Z_0)-\mu]^2}{2\zeta^2}\right]. \tag{4.1.8}$$

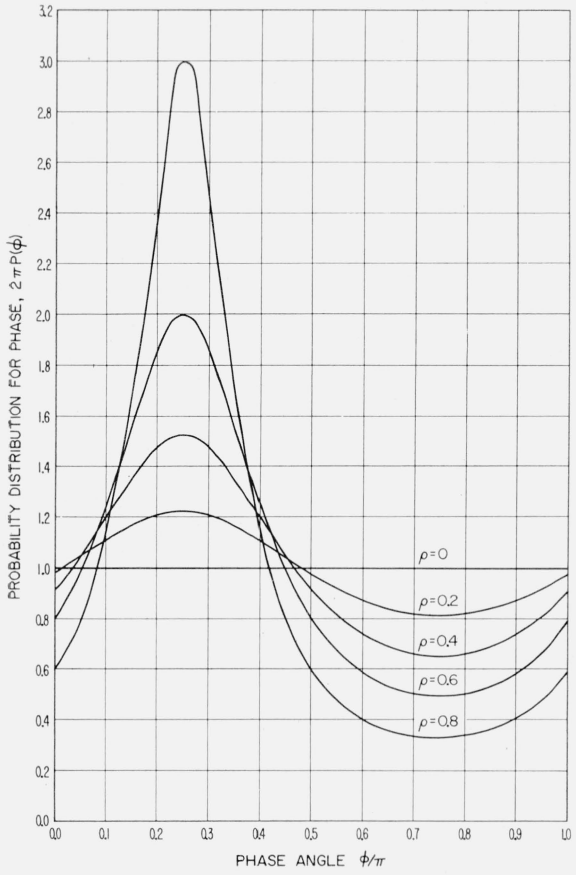

FIGURE 18. *Distribution of scatter signal phase angle ϕ for various cross correlations ρ.*

The corresponding short-term amplitude fluctuation must now be considered as a conditional probability density; that is, given σ or Z, the distribution of R is,

$$P(R|Z)=\frac{dRR}{Z}\log 4\exp-\left\{\frac{R^2\log 2}{Z}\right\}. \quad (4.1.9)$$

McCrossen [54] has evaluated the probability that R exceeds a fixed level r_0 at any instant, by integrating this expression over all possible values of Z, as well as $R>r_0$.

4.2. Electromagnetic Scattering

The basic field eq (3.2.3) for propagation through a turbulent medium also generates the solutions which describe propagation beyond the optical horizon. The single scattering (Born) approximation (3.2.4) is consistently used to describe scatter propagation [7, 45, 46]. E_0 is the field which would be received at $\vec{R}$ if there were no refractive irregularities, and is therefore the spherical earth diffraction field at points beyond the horizon. It has been established experimentally [47] that the scatter field strengths are many orders of magnitude greater than the diffracted fields 50 km beyond the horizon, so that E_0 must be omitted as the source of the scatter signals. This leaves the integral term in eq (3.2.4), which we have identified with single scattering of direct rays by the refractive blobs, as in figure 19a. The initial field E_0 is that which would be received at the scattering blob by line-of-sight propagation from the transmitter. The scattered wave proceeds from irregularity to receiver along the second (dashed) line-of-sight path, and is thus generically similar to the relay link problem characterized by figure 3a. The crucial difference lies in the scattering region V, which is now the common (wedge-shaped) volume defined by the intersection of tangent planes at the transmitter and receiver (see fig. 19a).

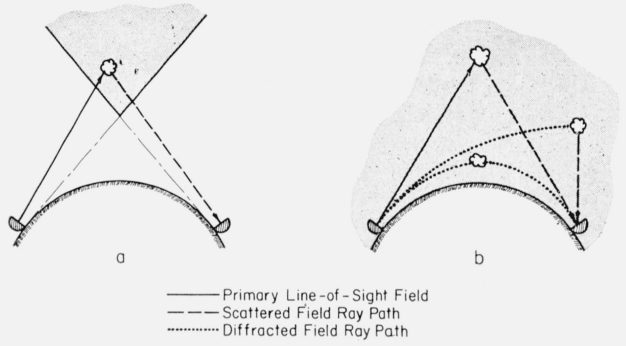

FIGURE 19. *Ray paths for scatter propagation: (a) Common (wedge) volume for line-of-sight ray paths, and (b) scattering of diffracted wave in shadow zone.*

The scattered field represented by the integral term in the Born approximation (3.2.4) gives rise to orthogonal signal components $x(t)$ and $y(t)$ which are in- and out-of-phase respectively relative to the comparatively weak phase reference E_0.

$$x+iy=FE_s=Fk_f^2\int_V d^3rG(\vec{R},\vec{r})\Delta\epsilon(\vec{r},t)E_0(\vec{r})\sin\chi, \quad (4.2.1)$$

F is the receiver gain factor,

$$F^2=A_R=\frac{\lambda^2G_R}{4\pi}$$

which transforms field strength (volts/cm) into receiver voltage (volts). We omit the polarization factor $\sin\chi$ for the time being. Separating (4.2.1) into real and imaginary components

$$x(t)=F\int_V d^3r\Delta\epsilon(\vec{r},t)\ \mathrm{Re}\left[-k_f^2G(\vec{R},\vec{r})E_0(\vec{r})\right],$$

$$y(t)=F\int_V d^3r\Delta\epsilon(\vec{r},t)\ \mathrm{Im}\left[-k_f^2G(\vec{R},\vec{r})E_0(\vec{r})\right], \quad (4.2.2)$$

completes the identification of voltage components in figure 16a and eq (4.1.1).

The variance and cross correlation of the orthogonal voltage components required in (4.1.2) can be established from these expressions using the spectrum method, as given by (2.3.1). Interchanging the orders of wavenumber (k) and scattering volume (r) integrations yields compact results similar to (3.4.1) in which the turbulence model $S(k)$ and geometrical considerations are explicitly separated.

$$\langle x^2\rangle=\frac{F^2}{8\pi^3}\int d^3kS(k)\left|\int_V d^3re^{i\vec{k}\cdot\vec{r}}\,\mathrm{Re}\left[k_f^2G(\vec{R},\vec{r})E_0(\vec{r})\right]\right|^2$$

$$\langle y^2\rangle=\frac{F^2}{8\pi^3}\int d^3kS(k)\left|\int_V d^3re^{i\vec{k}\cdot\vec{r}}\,\mathrm{Im}\left[k_f^2G(\vec{R},\vec{r})E_0(\vec{r})\right]\right|^2$$

$$\langle xy\rangle=\frac{F^2}{8\pi^3}\int d^3kS(k)\left\{\int_V d^3re^{i\vec{k}\cdot\vec{r}}\,\mathrm{Re}\left[k_f^2G(\vec{R},\vec{r})E_0(\vec{r})\right]\right\}$$
$$\times\left\{\int_V d^3re^{i\vec{k}\cdot\vec{r}}\,\mathrm{Im}\left[k_f^2G(\vec{R},\vec{r})E_0(\vec{r})\right]\right\} \quad (4.2.3)$$

The last integral is real in virtue of the Hermitian property of the spectrum $S^*(k)=S(-k)$, which follows from eq (2.3.1). The two basic scatter propagation integrals contained in (4.2.3) have not been evaluated explicitly to date. They have been attacked by the author at two levels of sophistication. The first method employs the simple common volume cutoff indicated by figure 19a. $E_0(r)$ is taken as a spherical wave expanding from the transmitter, and $G(R,r)$ is the free space Green's function of eq (3.2.5), representing unshielded expansion of the scattered wave from the blob to receiver. The common volume is then the wedge-shaped region described above and it is convenient to use rectangular coordinates centered on the wedge apex and the great circle plane between transmitter and receiver.

The second approach is indicated by figure 19b and recognizes the role of both line-of-sight and diffracted primary and/or scattered waves. In this case, one takes E_0 to be the actual (series) solution for a dipole radiating above a spherical conducting earth. This automatically includes line-of-sight propagation to blobs in the common volume, as well as blobs below the horizon which are reached only by the diffracted component of E_0. Subsequent propagation of the scattered radiation must also recognize the earth-screening effect, which is to say that the Green's function $G(R,r)$ must be that appropriate to the exterior of a conducting sphere. However, this is just the field due to a unit dipole placed at the scattering point, and is therefore given again by a series solution of the form used for E_0. This approach treats the three types of scatter paths shown in figure 19b exactly, and includes the scattering of diffracted waves and diffraction of scattered diffracted waves in a natural fashion. This refinement is probably of academic interest only, since Arons [55] has concluded that such effects are quite small for normal scatter circuits. This approach does have the advantage of treating height-gain effects and near horizon paths in a unified manner. The volume integrations in (4.2.3) required for this approach are not trivial and the surviving summations must be performed by the Watson transformation [56] in the end.

All of the precise development described above is essentially new and unpublished. The considerable theoretical literature on scatter propagation is based on the cross section approach which is built on a series of approximations to the integral representation (4.2.1) for the (complex) scattered field, and treats only the average scattered power $\langle R^2\rangle=\langle x^2\rangle+\langle y^2\rangle$. The first step is the far field approximation, which notes that the scattering blobs are always many, many wavelengths from both the transmitter and receiver (see, however, ref. 24). This allows the scalar distance between the receiver $\vec{R}$ and variable scattering point $\vec{r}$ to be expanded as follows:

$$\left|\overrightarrow{R_2-r}\right|\cong R_2-\frac{\vec{R}_2\cdot\vec{r}}{R_2}=R_2-\frac{\vec{k}_2\cdot r}{k_f} \quad (4.2.4)$$

where $\vec{k}_2$ is the propagation vector of the scattered wave ($|\vec{k}_2|=k_f=2\pi/\lambda$). The field E_0 incident on the point r is representable as,

$$E_0=\sqrt{\frac{P_TG_T}{4\pi}}\;\frac{1}{R_1}e^{i\vec{k}_1\cdot\vec{r}},$$

where $\vec{k}_1$ is the upgoing (line-of-sight) propagation vector. G_T is the gain of the transmitter along $\vec{k}_1$, and P_T is the transmitted power. Combining these expansions with (4.2.1) yields:

$$E_s\cong\frac{\pi}{\lambda^2}\sqrt{P_T}\,e^{ik_fR_2}\int_V d^3r\,\frac{e^{i\vec{r}\cdot\overrightarrow{(k_1-k_2)}}}{R_1R_2}\Delta\epsilon(\vec{r},t)\sqrt{\frac{G_T}{4\pi}} \quad (4.2.5)$$

The mean square received power is given in terms of receiver aperture $A_R=G_R\lambda^2/4\pi$ by

$$P_R=A_R\langle|E_s|^2\rangle=\frac{P_T}{16\lambda^2}\int d^3r\int d^3r'\langle\Delta\epsilon(\vec{r},t)\Delta\epsilon(\vec{r}',t)\rangle$$
$$\sqrt{G_RG_R'G_TG_T'}\;\frac{e^{i\vec{r}\cdot\overrightarrow{(k_1-k_2)}}e^{-i\vec{r}\cdot\overrightarrow{(k_1'-k_2')}}}{R_1R_2R_1'R_2'} \quad (4.2.6)$$

where k_1, k_2 and the gain functions are implicit functions of position. The second approximation is now invoked by noting that the space correlation in (4.2.6) vanishes unless the points $\vec{r}$ and $\vec{r}'$ are within several hundred meters of one another. The other factors in the integrand are relatively insensitive functions of position, so that

$$R_1=R_1',\ R_2=R_2',\ k_1-k_2=k_1'-k_2',\ G_T=G_T',\ G_R=G_R'$$

over the important joint regions of integration. By transforming to sum and difference coordinates,

$$r=r_1+r_2 \text{ and } \rho=r_1-r_2,$$

one can rewrite (4.2.6) as

$$P_R=\frac{P_T}{16\lambda^2}\int_V d^3r\,\frac{G_R G_T}{R_1^2 R_2^2}\int_V d^3\rho e^{i\vec{\rho}\cdot(\vec{k_1}-\vec{k_2})}\langle\Delta\epsilon^2\rangle C(\rho).$$

Because $C(\rho)$ is nonvanishing only over a small volume of ρ space, the ρ integration can be extended over all space without misrepresentation. The Fourier inverse of (2.3.1) then indicates that this (difference) integral is nothing more than the spectrum $S(k)$ evaluated at the uniquely important "scattering wavenumber",

$$K=|\overrightarrow{k_1-k_2}|=\frac{4\pi}{\lambda}\sin\theta/2, \tag{4.2.7}$$

where θ is the scattering angle formed by line-of-sight rays to the volume element d^3r,

$$P_R=\frac{P_T}{16\lambda^2}\int_V d^3r\,\frac{S\left[\left(\frac{4\pi}{\lambda}\sin\frac{\theta_r}{2}\right)\right]}{R_1^2R_2^2}G_T G_R. \tag{4.2.8}$$

This expression indicates that the scattering process selects those blobs in the hierarchy described by $S(k)$ whose wave numbers satisfy (4.2.7). This corresponds to constructive interference of the waves diffracted by the appropriate grating (i.e., blob) spacing for the Bragg angle θ. This selective isolation of only a certain size class of blobs is equivalent to the narrow band filter shown in figure 20 applied to the spectrum of irregularities.

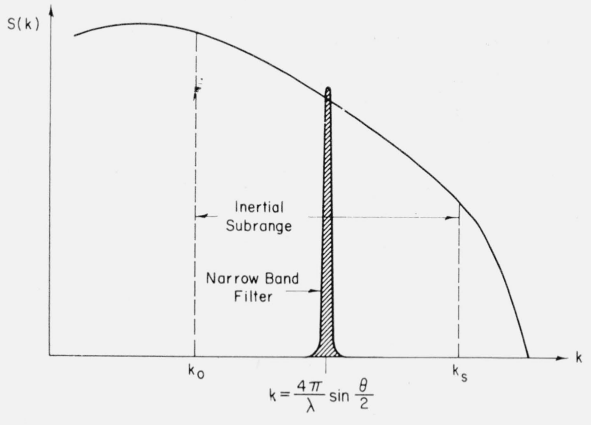

FIGURE 20. *Typical spectrum of refractive irregularities showing narrow band filter at the scattering wavenumber which characterizes tropospheric scattering.*

θ is the average scattering angle and λ is the radiation wave length.

The expression (4.2.8) for received power is often quoted in terms of a scattering cross section

$$\sigma(\theta,\lambda)=\frac{\pi^2}{\lambda^4}S\left(\frac{4\pi}{\lambda}\sin\frac{\theta}{2}\right). \tag{4.2.9}$$

This cross section measures the energy scattered per unit volume V, into a unit solid angle $d\omega$ which makes the angle θ with the initial Poyting vector S_0. This is illustrated in figure 21. The scattering cross section is always defined for a unit incident power, so that at a distance R from the scattering element V,

$$\sigma=\frac{R^2}{V}\left\langle\left|\frac{E_s(R)}{E_0}\right|^2\right\rangle, \tag{4.2.10}$$

which is equivalent to (4.2.9) in virtue of the Born approximation (4.2.1) for E_s. σ has the units cm^{-1}, since it is an ordinary cross section (cm^2) per unit volume (cm^{-3}).

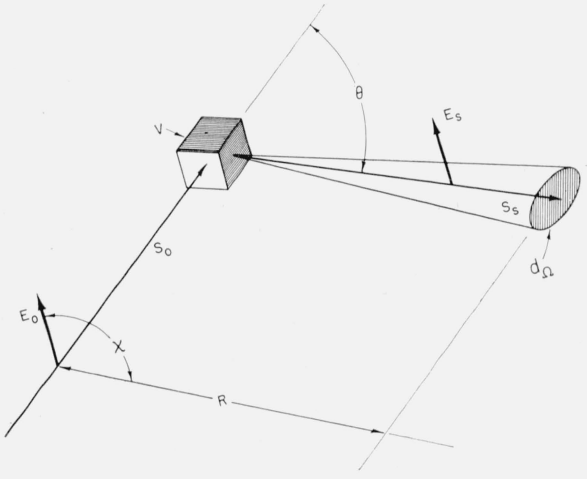

FIGURE 21. *Geometrical description of scattering cross section σ per unit volume and solid angle $d\Omega$ per unit incident power.*

The angular dependence of σ is often interpreted as the scattering polar diagram of an average blob. Reference to table 1 shows that almost all of the scattered radiation is projected into a small cone of beamwidth λ/l_0 about the forward direction. This means that scatter propagation circuits depend on the extremely weak side lobes of the scattering blobs, which explains, in part, why large dishes and high power are required to operate such links. Feshbach [57] has suggested that many small angle multiple scatterings could be more efficient than a single large angle scattering. Such effects certainly become increasingly important at frequencies above 1,000 Mc and/or very long paths, since the convergence of the Born series is related to the smallness of the equivalent line-of-sight rms phase variation computed along the equivalent (kinked) ray path eq (3.2.11) with $L\simeq d$. If this view is correct, the entire subject, which is summarized in subsequent

sections, requires revision. Further research should be directed to this interesting point.

The equivalence between σ and S given by eq (4.2.9) can be used to produce the familiar expression for received power $P_R \sim \langle R^2 \rangle$ to transmitted power $P_T \sim |E_0|^2$

$$\frac{P_R}{P_T} = \frac{\lambda^2}{16\pi^2} \int_V d^3r \, \frac{\sigma(\theta,\lambda)}{R_1^2 R_2^2} \, G_T G_R. \tag{4.2.11}$$

The corresponding spectrum integral is more fundamental, since the joint frequency-distance dependence is emphasized thereby.

$$\frac{P_R}{P_T} = \frac{1}{16\lambda^2} \int_V d^3r \, \frac{G_T G_R}{R_1^2 R_2^2} \, S\left(\frac{4\pi}{\lambda} \sin\frac{\theta}{2}\right) \tag{4.2.12}$$

Data taken with very narrow beams (see fig. 16b) is usually expressed in terms of this ratio.[6] If the beams are so narrow that the scattering angle, and hence the spectrum, is substantially constant over the common volume, the integration can be collapsed to

$$\frac{P_R}{P_T} \simeq \frac{V G_T G_R}{\lambda^2 d^4} \, S\left(\frac{4\pi}{\lambda} \sin\frac{\theta}{2}\right), \tag{4.2.13}$$

since $R_1 \simeq R_2 \simeq d/2$. The scattering volume is set by the aerial beamwidths β and the transmission distance d by $V \simeq 2(\beta d/4)^3/\theta$, where the average scattering angle is $\theta = d/a$ for $d \ll a$.

$$\frac{P_R}{P_T} \simeq \frac{\beta^3 G_T G_R}{32\lambda^2 d^2} \, S\left(\frac{2\pi d}{\lambda a}\right). \tag{4.2.14}$$

The majority of broad-beam data is given with respect to the free-space power P_{FS} which would be received over a line-of-sight path of the same length d.

$$\frac{P_{FS}}{P_T} = \frac{G_T}{4\pi d^2} \, \frac{\lambda^2 G_R}{4\pi}. \tag{4.2.15}$$

This measure of transmission efficiency emphasizes the loss which is due to the scattering propagation agency alone,

$$\frac{P_R}{P_{FS}} = \pi^2 d^2 \int_V d^3r \, \frac{1}{R_1^2 R_2^2} \, S\left(\frac{4\pi}{\lambda} \sin\frac{\theta}{2}\right). \tag{.16}$$

The receiver and transmitter gains also cancel in this expression, since they are relatively constant over the scattering volume. The equivalent expressions (4.2.12) and (4.2.16) will be used interchangeably in what follows.

[6] Additional factors of two are sometimes included [49] in such expressions to represent the addition of ground reflected waves. Our gain factors are defined to include all such effects.

4.3. Radiofrequency Dependence

The variation of received power with carrier frequency can be established without evaluating the difficult volume integrals presented in the last section. This is because the value of λ and θ relevant to most scatter paths combine to emphasize "scattering-wave numbers" which lie in the inertial range of the spectrum of tropospheric irregularities.[7] The physical models for $S(k)$ are proportional to simple inverse powers of k in the inertial range, and the radio-frequency dependence of the power ratio expressions (4.2.12) or (4.2.16) can be brought outside the integrals. If $S(k) = S_0 k^{-n}$, one has from (4.2.12),

$$\frac{P_R}{P_T} = \frac{\lambda^{n-2}}{16} \int_V d^3r \, \frac{G_T G_R}{R_1^2 R_2^2} \, \frac{S_0}{\left(4\pi \sin\frac{\theta}{2}\right)^n} \tag{4.3.1}$$

There is still a frequency dependence concealed in the gain functions, which is due to both wave length-dependent height gain factors and the absorbing area-gain relationship $G_R = A_R \, 4\pi/\lambda^2$. The ratio of received powers for scaled aerials on the same path is therefore

$$\frac{P_R(\lambda_1)}{P_R(\lambda_2)} = \left(\frac{\lambda_1}{\lambda_2}\right)^{n-4} \tag{4.3.2}$$

The mixing-in-gradient model (2.4.6) corresponds to $n=5$ and predicts a linear-wavelength dependence of scattered power. This prediction is in good agreement with careful analysis of the data from numerous broad-beam experiments when the role of height gain factors is carefully included [58]. The same model implies a λ^3 variation for the ratio P_R/P_T, which is quite consistent with narrow beam data [59]. It would appear that the $\lambda^{-0.33}$ dependence predicted by the Obukhov model (2.4.4) is not consistent with present radio data.

Bean [60] has studied the effect of tropospheric absorption on scatter signals as a function of frequency and distance, and finds that such effects do not influence the above conclusions. The variability of the frequency scaling exponent has been noted on all links, and one must be quite explicit about just which quantities are being compared on the two frequencies. It would seem that ratios of hourly means on the same path for the same hours would be the best choice of data, since [1] two widely separated frequencies do not fade together (see section 4.9), and [2] diurnal and seasonal effects may affect two frequencies differently. On the other hand, the NBS group finds that hourly medians on adjacent identical paths are not always the same, and a further examination of the problem is indicated. The above statements about frequency dependence refer to the average power, and hence to the average frequency exponent. It should be emphasized that it is this average value, and not the extreme values, [58, 61] which should be correlated with present (smoothed) experimental data.

[7] For example, if $f=1{,}000$ Mc and $d=400$ miles, $\lambda=1$ ft and $\theta=0.1$ radian eq (4.2.7) gives $K=2$ m^{-1}.

4.4. Distance Dependence

A large amount of experimental data on signal-power attenuation relative to free space drawn from reference [62] is plotted in figure 22. This is a heterogeneous sample of long-term medians, obtained in most cases with broad beam antennas. The data were taken during the wintertime, mostly in the afternoon, when tropospheric scatter is expected to be the dominant propagation mode. These data have not been normalized for the effects of radiofrequency, antenna heights, terrain or meteorological influences, which explains the considerable data scatter. If the observed linear wave-length dependence of the scatter signals is used to reduce these data to a common radiofrequency base, the data scatter is reduced. The empirical curve drawn through the data corresponds to an exponential variation of signal power at large distances, with approximately 0.1 db/mile. At shorter distances, the distance dependence is more complicated.

The distance dependence of scattered power is not as simple to extract as the radiofrequency variation. This is because such predictions depend upon careful integration of the spectrum's angular dependence over the common volume V, which, in turn, is defined by the transmission distance d. The gain factors are essentially constant in (4.2.12), so that the distance dependence of the mixing-in-gradient model (2.2.4) can be expressed in terms of the integral

$$P_R \simeq \int_V d^3r \, \frac{1}{R_1^2 R_2^2} \, \frac{\left(\frac{d\epsilon_0}{dh}\right)^2}{\left(\sin\frac{\theta}{2}\right)^5}, \qquad (4.4.1)$$

where all factors in the integrand depend on the great circle path distance d. The mixing-in-gradient model is subject to a more severe test than other models because it contains no (adjustable) turbulence parameters. The NBS group has used the meteorologically observed exponential variation of $d\epsilon_0/dh$ up to stratospheric heights to predict the experimental data presented in figure 22 quite well out to 700 miles [61, 62].

A substantial amount of early theoretical prediction [58, 63, 64] was based on height dependences assumed for the mean square dielectric fluctuation $<\Delta\epsilon^2> \propto h^{-n}$. This also increased the distance scaling law exponent by n and supplied some of the missing exponents for older correlation function models thereby. Insofar as one believes in the physical theories of mixing models, it is more realistic to insert measured profiles for $\epsilon_0(h)$ and let the theories be tested thereby.

In making precise comparisons between theory and experiment, it is necessary to recognize several important details. The effect of (irregular) terrain obstacles in modifying the takeoff angles, and hence the minimum scattering angle versus distance relation, led the NBS group to the concept of effective angular distance [58]. Refraction of the upgoing and downgoing beams by the mean profile ϵ_0 has been analyzed thus far by the equivalent earth radius method [58]. Bean [60] established theoretically the corrections due to tropospheric absorption on distance dependent scaling laws.

The simplest case to analyze is that for narrow-antenna beams, since the volume integration is then collapsed and approximated by eq (4.2.14). The

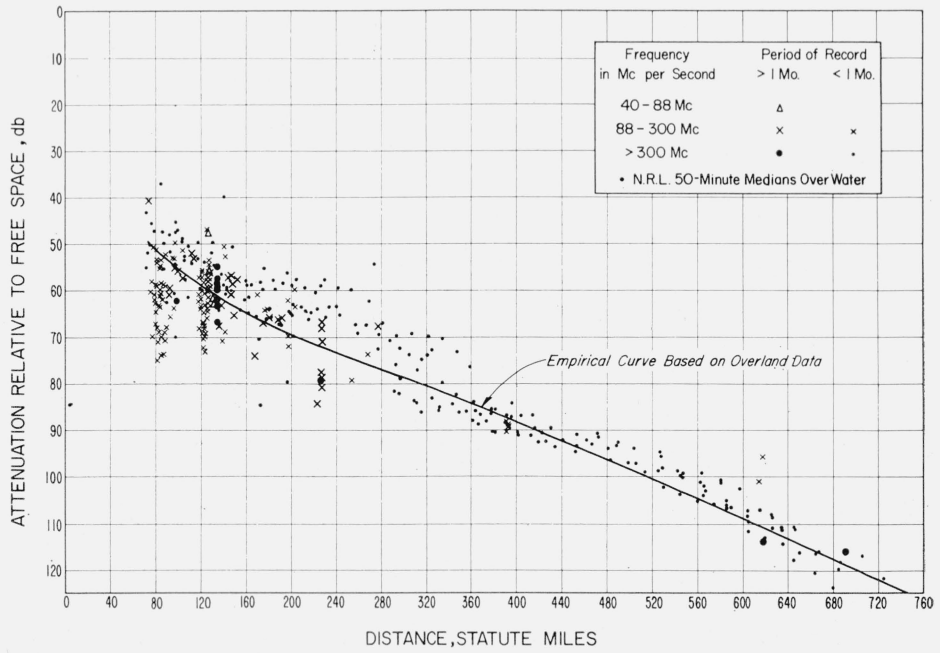

FIGURE 22. *Experimental data on distance dependence of tropospheric scatter field strength relative to free space for all frequencies, after Rice, Longley, and Norton* [62].

mixing-in-gradient model (2.4.6) predicts the following distance scaling law,

$$\frac{P_R}{P_T} \simeq \left[\frac{d\epsilon_0}{dh}\right]_V^2 \frac{\text{constant}}{d^7}, \tag{4.4.1}$$

for identical antennas and height gain effects. This result is independent of turbulent parameters, whereas the Obukhov model (2.4.4) gives

$$\frac{P_R}{P_T} \simeq \left[\frac{d\epsilon_0}{dh}\right]_V^2 \frac{k_0^{2/3}(V)}{d^{5.7}} \text{ constant}. \tag{4.4.2}$$

Both models depend upon the gradient of the mean profile ϵ_0 at the average scattering altitude. This point rises as the path length is increased and the gradient probably decreases accordingly. The narrow-beam data [65] suggests a scaling law of the form $1/d^9$, or possibly even $e^{-\xi d}$. Appropriate fitting of $d\epsilon_0/dh$ and/or k_0 in the foregoing can bring either theoretical result into agreement with almost any experimental scaling law, so that this type of measurement cannot be considered a very severe test of the theory at the present time.

4.5. Absolute Power Estimates

Probably the most difficult problem in scatter theory is to make reliable absolute power estimates. All of the explicit and implicit factors in (4.2.12) must be carefully evaluated. The following points must be recognized in reaching accurate power predictions: (a) Horizon limitations of local terrain, (b) height gain effects in the antennas, (c) lobe patterns of the antennas, (d) variation of dielectric irregularity intensity with height, (e) refraction of primary and scattered rays, (f) absorption, (g) anisotropy influences, and (h) transmitter and receiver antenna loading.

The problem has only been solved completely by the NBS group, using numerical techniques [61, 62]. They considered broad-antenna patterns with the mixing-in-gradient model and obtained good (absolute) agreement with experimental data.

The problem is primarily one of finding a judicious coordinate system in which to perform the complicated volume integration of (4.2.12). The NBS spherical system [66] can be integrated exactly for many turbulence models [67], but is not adaptable to height-dependent scattering cross sections. The rectangular system used by Staras [64] circumvents this problem, but relies on approximations which are difficult to assess. It is anticipated that the precise integration schemes suggested by eq (4.2.3) will supply an accurate means for making absolute power level comparisons. A height-dependent factor $(d\epsilon_0/dh)^2$ in the spectrum enters into (4.2.3) as a factor $d\epsilon_0/dh$ in each fundamental integral.

An important achievement for scatter theory is the reliable prediction of signal strengths beyond the horizon from surface measurements of $(d\epsilon_0/dh)_0$ at the earth's surface [62]. This means that diurnal and seasonal (relative) variations of scattered power can be anticipated without recourse to complicated volume integrations, since the gradient profile,

$$\frac{d\epsilon_0}{dh} = \left[\frac{d\epsilon_0}{dh}\right]_0 F(h), \tag{4.5.1}$$

permits the time-variable ground level factor to be removed from the geometrical integrals.

4.6. Amplitude Stability of Scatter Signals

The characteristic random fading of the amplitude of scatter signals is of considerable practical importance, since useful information can only be transmitted when the signal strength is above a fixed level. The temporal variations of the signal envelope are physically related to the incoherent addition of (random) Doppler-shifted waves received from different elements of the scattering volume. A typical time record of scatter signals is shown in figure 23, together with the time-displaced vector voltage diagrams corresponding to the instants t_1 and t_2. The basic theoretical problem is to predict the joint probability that the signal amplitude will assume the values R_1 and R_2 at times separated by an interval $\tau = t_2 - t_1$. The average time between maxima and zero crossings, amplitude auto correlations, etc., can all be computed from such a result.

The purely statistical descriptions of fading must be discussed first. The distribution of time-displaced signal amplitudes shown in figure 23 depends on the four dimensional probability density for the set (x_1, y_1, x_2, y_2). Since the individual orthogonal signal components $x(t)$ and $y(t)$ are considered to be distributed in a Gaussian manner at each instant, the required density is a four dimensional Gaussian multivariate form,

$$P(Z_i) = \frac{1}{4\pi^2 |M|} \exp -\frac{1}{2} \sum_1^4 \sum_1^4 Z_i Z_j M_{ij}^{-1} \tag{4.6.1}$$

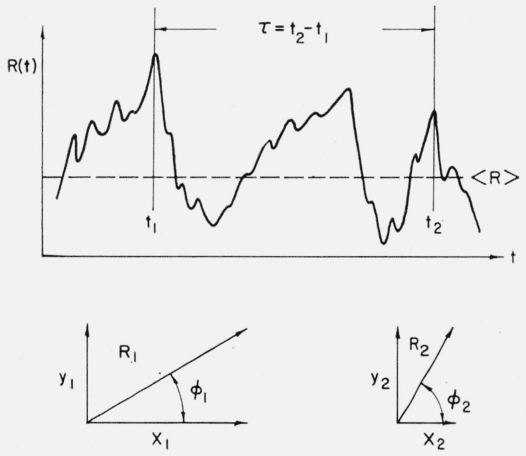

FIGURE 23. *Typical time record of randomly fading scatter signal amplitude with corresponding time-displaced vector voltage diagrams.*

⟨R⟩ is the average amplitude and ϕ is the instantaneous phase of the signal.

where $Z_1=x(t)$, $Z_2=y(t)$, $Z_3=x(t+\tau)$, $Z_4=y(t+\tau)$. The moment matrix M_{ij} is the basic characterization [8] of the fading signal.

$$M=\begin{bmatrix} \langle x^2(t)\rangle & \langle x(t)y(t)\rangle & \langle x(t)x(t+\tau)\rangle & \langle x(t)y(t+\tau)\rangle \\ \langle x(t)y(t)\rangle & \langle y^2(t)\rangle & \langle x(t+\tau)y(t)\rangle & \langle y(t)y(t+\tau)\rangle \\ \langle x(t+\tau)x(t)\rangle & \langle x(t+\tau)y(t)\rangle & \langle x^2(t+\tau)\rangle & \langle x(t+\tau)y(t+\tau)\rangle \\ \langle x(t)y(t+\tau)\rangle & \langle y(t)y(t+\tau)\rangle & \langle x(t+\tau)y(t+\tau)\rangle & \langle y^2(t+\tau)\rangle \end{bmatrix} \qquad 4.6.2$$

The matrix M_{ij} is symmetrical because the component processes are assumed to be stationary. The cylindrical transformations $x=R\cos\phi$ and $y=R\sin\phi$ which define the signal amplitude and phases (see fig. 23) must be inserted into expression (4.6.1) to establish the time-displaced phase and amplitude distribution. This portion of the problem is analytically very complicated unless the moment matrix M_{ij} assumes especially simple forms, and it is desirable to investigate the time correlations themselves before pursuing the statistical problem further.

The propagation problem is to compute the moment matrix of eq (4.6.2) explicitly. This has not been done. One can, however, establish general expressions for the time-displaced correlations [9] in M_{ij} by using the integral representations for $x(t)$ and $y(t)$ established previously from the Born approximation (4.2.2), viz,

$$x(t)=\int_V d^3r\Delta\epsilon(r,t)H(r),$$

$$y(t)=\int_V d^3r\Delta\epsilon(r,t)J(r), \qquad (4.6.3)$$

where $H(r)$ and $J(r)$ are the real and imaginary parts respectively of the complex product $[k^2G(R,r)E_0(r)]$ in eq (4.2.2). The appropriate averages can now be computed using the integral representation (2.5.2) for the space- and time-displaced correlation of dielectric fluctuations.

$$\langle x(t)x(t+\tau)\rangle=\int_V d^3rH(r)\int_V d^3r'\,H(r')\langle\Delta\epsilon(r,t)\Delta\epsilon(r',t+\tau)\rangle$$

$$=\frac{1}{(2\pi)^3}\int d^3k\,S(k)\eta\,[k,\tau]e^{-i\vec{k}\cdot\vec{U}\tau}\left|\int_V d^3rH(r)e^{i\vec{k}\cdot\vec{r}}\right|^2$$

$$\langle y(t)y(t+\tau)\rangle=\frac{1}{(2\pi)^3}\int d^3k\,S(k)\eta(k,t)\,e^{-i\vec{k}\cdot\vec{U}\tau}\left|\int_V d^3rJ(r)\,e^{i\vec{k}\cdot\vec{r}}\right|^2$$

$$\langle x(t)y(t+\tau)\rangle=\langle x(t+\tau)y(t)\rangle$$

$$=\frac{1}{(2\pi)^3}\int d^3k\,S(k)\eta(k,t)\,e^{-i\vec{k}\cdot\vec{U}\tau}\left(\int_V d^3rH(r)e^{i\vec{k}\cdot\vec{r}}\right)\left(\int_V d^3r'J(r')e^{-i\vec{k}\cdot\vec{r}'}\right) \qquad (4.6.4)$$

The important point to note here is that the geometrical integrals involving $H(r)$ and $J(r)$ are precisely those required for the same-time calculations of signal properties. Although these integrals have not been evaluated to date, it is significant that the two-time problem is no more difficult than the same-time problem as far as the propagation calculations are concerned.

The statistical problem has been treated heretofore [51, 69] by assuming very special forms for the moment matrix.

$$\langle x_1^2\rangle=\langle x_2^2\rangle=\langle y_1^2\rangle=\langle y_2^2\rangle=\sigma^2$$
$$\langle x_1x_2\rangle=\langle y_1y_2\rangle=\sigma^2\mu(\tau) \qquad (4.6.5)$$

$\mu(\tau)$ is here called the basic propagation correlation coefficient. All cross correlations are assumed to vanish identically. The joint probability density (4.6.1) now reduces to a comparatively simple form, which is readily transformed into the polar amplitude-phase coordinates of figure 23,

$$P[R_1,R_2,\phi_1,\phi_1;\tau]=\frac{R_1R_2}{4\pi^2\sigma^4(1-\mu^2)}$$
$$\exp-\left[\frac{R_1^2+R_2^2-2\mu R_1R_2\cos(\phi_1-\phi_2)}{2\sigma^2(1-\mu^2)}\right] \qquad (4.6.6)$$

The joint amplitude distribution for R_1 and R_2 is obtained by integrating this expression over both phase angles.

$$P[R_1,R_2;\tau]=\frac{R_1R_2}{\sigma^4(1-\mu^2)}\,I_0\left[\frac{\mu R_1R_2}{\sigma^2(1-\mu^2)}\right]e^{\frac{R_1^2+R_2^2}{2\sigma^2(1-\mu^2)}} \qquad (4.6.7)$$

[8] $|M|$ is the determinant of M_{ij} and M_{ij}^{-1} its inverse.

[9] The one-time components are special cases of the time-displaced correlations, e.g., $\langle x(t)y(t)\rangle=\langle x(t)y(t+\tau)\rangle_{\tau=0}$.

The amplitude autocorrelation can be expressed in terms of complete elliptic functions,

$$\langle R(t)\,R(t+\tau)\rangle=\langle R_1R_2\rangle=\sigma^2\{2E(\mu)-(1-\mu^2)K(\mu)\} \tag{4.6.8}$$

and is plotted in figure 24 as a function of $\mu(\tau)$. For large time separations (i.e., μ small), this result approaches the square of the average amplitude, $\langle R\rangle^2=\frac{\pi}{2}\sigma^2$. For small separations or μ near unity, it approaches $\langle R^2\rangle=2\sigma^2$. The frequency spectrum of amplitude variations can be obtained from (4.6.8) by the Fourier cosine transformation, if $\mu(\tau)$ is known explicitly as a result of propagation calculations.

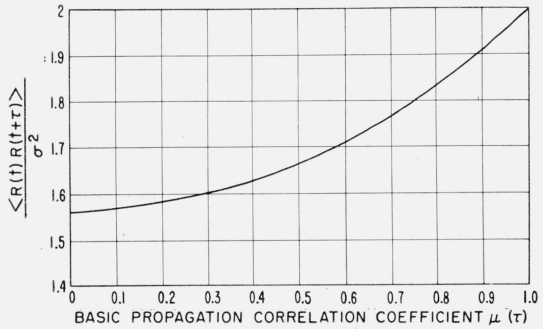

FIGURE 24. *Normalized autocorrelation of scatter signal amplitude versus basic propagation correlation coefficient* $\mu(\tau)$.

The envelope fading rate, or average number of positive crossings of the median signal level R per unit time in figure 23, is a convenient measure of the time-varying random signal. This fading rate N can be identified in the small argument expansion of the amplitude autocorrelation [30].

$$\langle R(t)\,R(t+\tau)\rangle=\langle R^2\rangle[1-\tfrac{1}{2}(\pi N\tau)^2\ \ldots\ ]. \tag{4.6.9}$$

If the basic propagation correlation coefficient $\mu(\tau)$ has a similar expansion,

$$\mu(\tau)=1-\tfrac{1}{2}[\gamma\tau]^2\ \ldots \tag{4.6.10}$$

Reduction of expression (4.6.8) leads to the following relationship:

$$N=\frac{\gamma}{\sqrt{2}} \tag{4.6.11}$$

The basic propagation problem is to predict the radiofrequency and distance dependence of γ.

Early studies of fading rates on scatter links recognized that the primary fading mechanism was due to Doppler-shifting of the signal by motion of the scattering medium. An rms sum of the drift velocity U and average eddy velocity V_0 was imagined to give the effective speed [32, 68]

$$N=\frac{f}{c}\left[\left(2U\,\mathrm{Sin}\,\frac{\theta}{2}\right)^2+\frac{1}{3}\,V_0^2\right]^{\frac{1}{2}}, \tag{4.6.12}$$

where θ is the average scattering angle in the common volume. The linear frequency dependence is characteristic of simple Doppler-shifting.

The geometry of a broad-beam scatter link shown in figure 25 indicates, however, that the situation is rather more complicated [69]. Consider first the midpoint (A) in the scattering volume. Since Doppler shifts are only caused by net elongation (or contraction) of the propagation path, the predominantly horizontal drift will cause no fading of the signal scattered from midpoints. On the other hand, the smaller random velocity V_0 has an arbitrary direction and can impose Doppler shifts on this component of the scattered signal. Consider next an offcenter scattering element (B). The drift velocity U now has a small component $U_\perp$ which bisects the propagation paths, and therefore does impose a Doppler shift. The fading contribution of these off-axis blobs is small because: (*i*) $U_\perp$ is a small projection of U, and (*ii*) the power scattered from point B is considerably smaller than that from point A due to the larger scattering angle θ'. Direct confirmation of this prediction was obtained by the Lincoln Laboratory Group [59], who noted that the fading rate decreased when very narrow-antenna beams are swung simultaneously away from the path midpoint A.

A considerable advance in analyzing this fading phenomenon was made recently by using the spectral representation of the turbulent dielectirc fluctuations [14]. The explicit separation of drift and random velocity contribution to the space-time correlation of $\Delta\epsilon$ in eq (2.5.2) suggests the following time-displaced generalization of the cross section result (4.2.12),

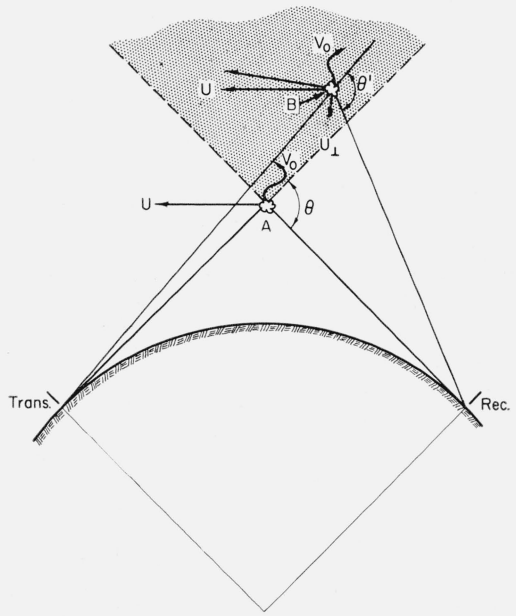

FIGURE 25. *Geometrical description of doppler shifts imposed by horizontal drift speed* $\vec{U}$ *and random velocity* $\vec{V}_0$ *at: (A) Path midpoint, and (B) off axis scattering volume elements.*

$$\langle R(t)R(t+\tau)\rangle \simeq \int_V d^3r S(|\vec{K}|)\, e^{i\vec{K}\cdot\vec{U}\tau\eta}\,[V_0 k_0^{1/3}|\vec{K}|^{2/3}\tau], \tag{4.6.13}$$

where $\vec{K}$ is the scattering difference vector defined by (4.2.7). Since the major component of the drift speed is usually horizontal, and therefore perpendicular to $\vec{K}$ for midpoint scattering, the significant contribution of drift is made by volume elements far from the midpoint. The random self motion V_0 has no such projection factor and contributes throughout the scattering volume. Expansion of (4.6.13) in a power series of τ and identification with expression (4.6.9) indicates that the fading rate due to self-motion is proportional to $f^{2/3}$, while drift motion gives the usual linear Doppler dependence on frequency. Available data indicates a variable frequency exponent less than one [32], so that some mixture of the two effects is indicated. Further experimental results are needed, especially data on the distance-dependence of N. The theory needs to be clarified by evaluating $\mu(\tau)$ from eq (4.6.4) for several propagation models.

4.7. Phase Stability of Scatter Signals

The phase stability of scatter signals has received little attention to date—either theoretically or experimentally. The question is potentially quite interesting because of the possibility of passing stable frequency references beyond line-of-sight by this mode. Frequency excursions about a single carrier are completely equivalent to time rates of change of the signal phase $\phi(t)$ defined in figure 23. The mean frequency change is thus given in terms of the autocorrelation of phase

$$\langle \delta f^2\rangle = \langle \dot{\phi}(t)\dot{\phi}(t+\tau)\rangle\Big|_{\tau=0} = -\frac{d^2}{d\tau^2}\langle \phi(t)\phi(t+\tau)\rangle\Big|_{\tau=0}. \tag{4.7.1}$$

The relative change in phase between two instants,

$$\langle |\phi(t)-\phi(t+\tau)|^2\rangle \simeq 2[\langle\phi^2\rangle - \langle\phi(t)\phi(t+\tau)\rangle], \tag{4.7.2}$$

is independent of the absolute path phase reference, and is probably easier to measure experimentally.

The central quantity in such studies is the autocorrelation of phase taken between two instants. For the special assumptions indicated by (4.6.5), it is possible to derive this result in terms of the basic propagation correlation coefficient $\mu(\tau)$. Integrating (4.6.6) over the amplitudes R_1 and R_2 gives the distribution for ϕ_1 and ϕ_2 deduced by Bunimovich [70]

$$P[\phi_1,\phi_2;\tau] = \frac{(1-\mu^2)}{4\pi^2}\left[\frac{1}{1-\omega^2} + \omega\,\frac{\frac{\pi}{2}+\sin^{-1}\omega}{(1-\omega^2)^{3/2}}\right] \tag{4.7.3}$$

where $\omega = \mu\cos(\phi_1-\phi_2)$. Wagner [10] has used this result to calculate the phase autocorrelation,

$$\langle \phi(t)\phi(t+\tau)\rangle = \frac{\pi}{2}\sin^{-1}\mu + \frac{1}{2}[\sin^{-1}\mu]^2 - \pi\int_0^{\pi/2} dx[\sin^{-1}(\mu\cos x)]^2 \tag{4.7.4}$$

and this is plotted in figure 26 versus $\mu(\tau)$. For very large τ or μ small, the phases are completely uncorrelated. For μ unity, expression (4.7.4) approaches the mean square value $\langle\phi^2\rangle = \pi^2/3$.

It is interesting that the phase correlation can be inferred from experimental data on amplitude correlations, since μ is only a parameter which may be eliminated between eq (4.6.7) and (4.7.4). When the more general moment matrix (4.6.2) is used, however both results will depend on two or more basic functions of τ. In that case, it is still possible to convert phase into amplitude data and vice versa by eliminating τ, although one must first complete explicit progagation calculations for $\mu(\tau)$, etc.

4.8. Space Correlation and Diversity Reception

A combination of two or more spaced receivers is frequently exploited to overcome signal loss during deep fades. This diversity reception depends upon spacing the antennas sufficiently far apart to insure independent fading of the two signals. The best experimental data available is that taken at 1,046 Mc by the NBS group [72]. The statistical problem is very similar to that illustrated in figure 26, if one reinterprets R_1 as the instantaneous signal amplitude induced in the first receiver and R_2 that induced in the second, at the same instant. The joint probability density for R_1 and R_2 is given by eq (4.6.7), if the basic correlation coefficient $\mu(D)$ is now the space correlation between the orthogonal signal components at the two receivers. Staras [73] computed the probability that the greater of the two (diversity) signals is above a specified level, as a function of the correlation coefficient μ (D). These statistical predictions have been checked against experimental data [74] and seem to fit quite well.

The propagation problem is to estimate the space coefficient μ (D). Gordon [63] and Rice [68] presented qualitative analysis which showed that the correlation distance normal to the propagation path

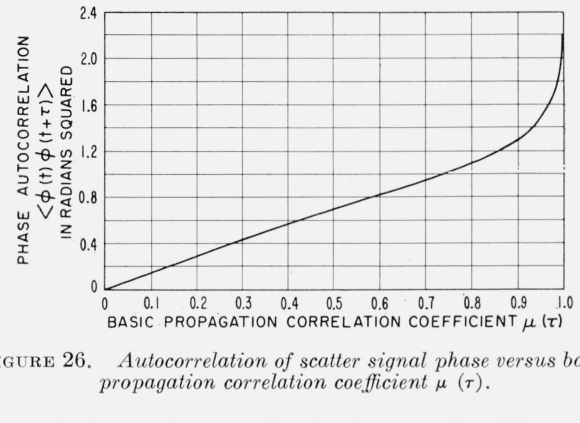

FIGURE 26. *Autocorrelation of scatter signal phase versus basic propagation correlation coefficient* μ (τ).

[10] R. J. Wagner, to be published.

(horizontal and vertical) ought to be of the order $\lambda a/d$, where d is the transmission distance and a the radius of the earth. A correlation distance $\lambda a^2/d^2$ along the path was also estimated. The RCA experiments [74] at 390 Mc for path lengths of 73 and 153 miles, however, failed to show the predicted decrease of horizontal and vertical correlation lengths with path distance. On the other hand, the simple wavelength dependence of these results is borne out by multiple frequency experiments [53, 75].

Analytical propagation calculations of all three correlation functions[11] as functions of receiver separation distance were derived by Staras [64], using the exponential space correlation model. His results have the same form as Gordon's, but are numerically different by substantial factors. Staras also included the effects of anisotropy in the refractive irregularities and found that this affected the predicted horizontal (transverse) correlation distance,

$$S=\frac{1.4\pi}{r}\left(\frac{a}{d}\right)\lambda, \qquad (4.8.1)$$

where r is the vertical-to-horizontal scale length ratio. By fitting data taken on 100 and 1000 Mc [53, 72] he suggested that this ratio should be about 0.25. Such comparisons are important in that they bear directly on the question of anisotropy, but more good data is needed.

The realization of plane-earth height-gain advantages is limited by space coherence between the actual receiver and its image. The usual height-gain curve is realized if the antenna is less than one-half the vertical correlation distance ($\lambda a/2d$). Only slight improvement is gained above this height by the gradual decrease of the scattering angle.

4.9. Frequency Correlation and Medium Bandwidth

The signal-frequency bandwidth which the scatter medium can support without serious distortion is intimately related to the multipath delays which are experienced. These depend upon the size of the effective scatter volume, which in turn is determined by the antenna bandwidths and/or the scattering pattern of the blobs. When the antenna patterns (β) are broad, the multipath is controlled by the scattering blobs and the approximate result of Gordon [63] predicts that

$$\Delta f=\frac{5ca^2}{d^3}, \qquad \beta>>\frac{d}{a} \qquad (4.9.1)$$

or numerically

$$\Delta f_{\mathrm{Mc}}=30/d^3,$$

where d is in hundreds of miles. This result shows that the bandwidth decreases rapidly with distance. Rice's estimate [68] of Δf varies inversely with the path length d, but is based on an oversimplified physical model.

A real improvement in bandwidth capabilities is obtained with very narrow beams. Although some antenna gain degradation is experienced with narrow beams, the angular distribution of multipath signals which are admitted to the receiver is reduced and the bandwidth thereby increased. Booker and de Bettencourt [76] examined this problem for beams narrower than the average scattering angle $\bar{\theta}=d/a$ and found

$$\Delta f=\frac{4ca}{\beta d^2}, \qquad \beta<<\frac{d}{a} \qquad (4.9.2)$$

This result indicates steady improvement with antenna size and decreases less rapidly with distance than (4.9.1). When aircraft fly through the path, the solid bistatic reflections from them supply a multipath signal of unusual magnitude and the above estimates for broad-antenna beams are meaningless.

Figure 27 indicates typical successive plots of amplitude versus frequency, such as might be obtained by sweeping a narrow-band transmitter about the carrier f_0. The joint amplitude distribution (4.6.7) can be used to describe this situation if R_1 is interpreted as the signal strength at f_0 and R_2 that at $f_0+\Delta f$. The basic correlation function μ is now a function of the frequency separation Δf and other propagation variables. If the correlation is high, it means that the signal components at either end of the frequency band being used are behaving essentially in unison, and little or no distortion is expected. Staras [64] evaluated substantially this function directly for omnidirectional antennas with

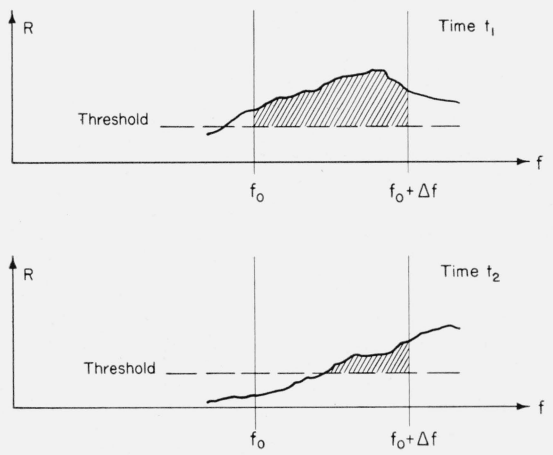

FIGURE 27. *Typical successive amplitude records plotted versus carrier frequency over a band Δf.*

The receiver threshold level indicates the role of absolute power level in correlation comparisons.

[11] Along, horizontally normal (transverse), and vertically normal to the propagation path.

the exponential space correlation model, and finds that the frequency correlation drops to 0.5 when

$$\Delta f_{mcs}=\frac{4}{d^3} \tag{4.9.3}$$

where d is in hundreds of miles. Reference to figure 24 indicates that (4.9.3) refers also to the envelope (R) correlation, so a factor of eight difference exists between (4.9.1) and (4.9.3). This problem evidently requires further clarification and careful comparison with experimental data. It is possible to use the spectral separation of turbulence and propagation effects indicated by (4.6.4) to calculate the frequency correlation coefficient $\mu(\Delta f)$. One need only evaluate the results of the frequency-dependent geometric integrals at displaced frequencies and set $\tau=0$ in (4.6.4).

The published experimental data has been taken with narrow-antenna beams, and is therefore not directly useful in resolving the theoretical conflict. The recent Lincoln Laboratory data [77] measures the frequency correlation in the manner of figure 27, by using a rapid frequency-change system. Their results indicate that signals separated by 2 Mc at 2,300 Mc over a 188-mile path give an amplitude correlation of 0.4. This is consistent with the television experiments of Tidd [78] on a similar path at 5,000 Mc.

It is important to note that the receiver threshold level influences the apparent bandwidth of a system. Figure 27 indicates how amplitude fading at time t_2 can reduce the frequency band over which the signal is correlated with the proceeding signal. This has lead to the concept of "instantaneous bandwidth," which finds application in designing efficient modulation systems to work with the scatter propagation mode.

4.10. Gain Loss or Antenna-to-Medium Coupling

When very narrow beams are used on scatter circuits, it is found that free-space antenna gains are not realized. This is known as gain loss or antenna-to-medium coupling loss and arises from the fact that signals arrive at the receiver from an extended scattering volume V. Narrowing the antenna beam eventually reduces this common volume faster than the aerial gain is increased (see fig. 16b) so that a relative gain loss is incurred.

Booker and de Bettencourt [76] analyzed this problem for similar conical antenna patterns at the transmitting and receiving ends of the circuit. They argued that no gain loss should be incurred so long as the beamwidth β is greater than $\frac{2}{3}d/a$. When the beams are sharper than this average scattering angle, they suggest that a relative power loss factor

$$L=0.43\left(\frac{d}{\beta a}\right)^3, \tag{4.10.1}$$

will be incurred. They point out that this result is probably too large because the height dependence of $\langle\Delta\epsilon^2\rangle$ was neglected and sharp beams were employed. The calculations by Nortion, Rice, and Vogler [58] used an exponential correlation function and an inverse square height dependence of $\langle\Delta\epsilon^2\rangle$. Staras [79] treated anisotropic irregularities and dissimilar antenna patterns. His results are between 5 and 8 db less severe than these predictions by Booker and de Bettencourt, and seem to give rather good agreement with experimental data.

Hartman and Wilkerson [80] have reinvestigated the problem, using an exponential decrease of isotropic turbulent fluctuations with height. Their calculations produce gain loss estimates which are several decibels less than those predicted by Staras, and in good agreement with considerable experimental data.

4.11. Beam Swinging

It is found experimentally that the scatter signal amplitude decreases when narrow beamwidth antennas are jointly swung off the great circle path, or simultaneously elevated as shown in Figure 28. For azimuth swinging, the effect is simply to increase the average scattering angle θ between the ray paths (beams) [81]. This reduces the scattered power because of the large exponent of $\sin\theta/2$ in the various scattering cross section expressions (see sec. 4.2).

Booker and de Bettencourt [76] analyzed the effect of swinging the transmitting and receiving aerials simultaneously in azimuth and elevation. They used a height-independent exponential correlation to make estimates of this power reduction, which are apparently in good agreement with available data.

The dependence of power loss on elevation swinging must also recognize the observed decrease of turbulent intensity with height. Since $\langle\Delta\epsilon^2\rangle$ probably decreases exponentially with height, the concomitant scattering height change Δh can effect the power levels significantly if it is comparable with the atmospheric scale height $H=22{,}000$ ft. The problem evidently needs further analysis and comparison of theory and experiment.

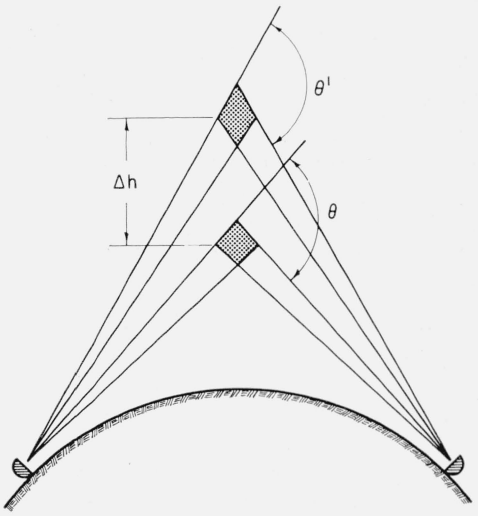

FIGURE 28. *Geometry for vertical beam swinging experiment showing increased scatter angle and higher common volume.*

The preparation of this paper is due in large part to the hospitality extended by the Boulder Laboratories of the NBS and to invaluable discussions with my colleagues there. W. Hartman and E. Barrows of that laboratory were particularly helpful in bringing the paper to final form and checking the analytical results.

5. References

[1] C. M. Crain, Survey of airborne microwave refractometer measurements, Proc. I.R.E. **43,** 1405 (1955).

[2] G. Birnbaum and H. E. Bussey, Amplitude, scale and spectrum of refractive index inhomogeneities in the first 125 meters of the atmosphere, Proc. I.R.E. **43,** 1412 (1955).

[3] M. C. Thompson and H. B. Janes, Measurements of phase stability over a low-level tropospheric path, J. Research NBS **63D,** 45 (1959).

[4] Albert D. Wheelon, Relation of radio measurement to the spectrum of tropospheric dielectric fluctuations J. Appl. Phy. **28,** 684 (1957).

[5] D. Mintzer, Wave propagation in a randomly inhomogeneous medium, J. Acoustical Soc. Am. I: **25,** 922 (1953), II:**25,** 1107 (1953), III:**25,** 186 (1954).

[6] H. G. Booker and W. E. Gordon, The role of stratospheric scattering in radio communication, Proc. I.R.E. **45,** 1223 (1957).

[7] F. Villars and V. F. Weisskopf, The scattering of electromagnetic waves by turbulent atmospheric fluctuations, Phys. Rev. **94,** 232 (1954).

[8] F. Villars and W. F. Weisskopf, On the scattering of radio waves by turbulent fluctuations of the atmosphere, Proc. I.R.E. **43,** 1232 (1955).

[9] A. M. Obukhov, Structure of the temperature field in turbulent flow, Izvest. Akad. Nauk S.S.S.R. Ser. Geofiz. **13,** 58 (1949).

[10] R. A. Silverman, Turbulent mixing theory applied to radio scattering, J. Appl. Phys. **27,** 699 (1956).

[11] R. Bolgiano, The role of turbulent mixing in scatter propagation, IRE Trans. PGAP **6,** 159 (1958).

[12] Albert D. Wheelon, Spectrum of turbulent fluctuations produced by convective mixing of gradients, Phys. Rev. **105,** 1706 (1957). (See also J. Geophys. Research **62,** 93 (1957), Radio frequency and scattering angle dependence of ionospheric scatter propagation at VHF, et seq.)

[13] B. R. Bean and F. M. Meaney, Applications of the monthly median refractivity gradient in tropospheric propagation, Proc. I.R.E. **43,** 1419 (1955).

[14] R. A. Silverman, Fading of radio waves scattered by dielectric turbulence, J. Appl. Phys. **28,** 506 (1957).

[15] W. Heisenberg, Zur statistischen theorie der turbulenz, Z. physik. **124,** 628 (1948).

[16] C. F. Von Weizsacker, Das spektrum der turbulenz bei grossen Reynolds'schen zahlen, Z. physik. **124,** 614 (1948).

[17] G. Munch and A. D. Wheelon, Space-time correlations in stationary isotropic turbulence, Phys. Fluids **I,** 462 (1958).

[18]. S. O. Rice, Mathematical analysis of random noise, BSTJ, **24,** 46, 100 et seq. (1945).

[19] K. A. Norton, L. E. Vogler, W. V. Mansfield, and P. J. Short, The probability distribution of the amplitude of a constant vector plus a Rayleigh-distributed vector, Proc. I.R.E. **43,** 1354 (1955).

[20] H. Bremmer, On the theory of fading properties of a fluctuating signal imposed on a constant signal, NBS Circ. 599 (May 1959).

[21] K. A.Norton, E. L. Schultz, and H. Yarbrough, The probability distribution of the phase of the resultant vector sum of a constant vector plus a Rayleigh-distributed vector, J. Appl. Phys. **23,** 137 (1952).

[22] J. R. Johler, and L. C. Walters, The mean absolute value and standard deviation of the phase of a constant vector plus a Rayleigh-distributed vector, J. Research NBS **62,** 183 (1959) RP2950.

[23] Albert D. Wheelon, Near-field corrections to line-of-sight propagation, Proc. I.R.E. **43,** 1459 (1955).

[24] M. Balser, Some observations on scattering by turbulent inhomogeneities, IRE Trans. PGAP **AP-5,** 383 (1957).

[25] S. Stein, Some observations on scattering by turbulent irregularities, IRE Trans. PGAP **AP-6,** 299 (1958).

[26] T. H. Ellison, The propagation of sound waves through a medium with very small random variations in refractive index, J. Atmospheric and Terrest. Phys. **2,** 14 (1951).

[27] S. M. Rytov, Light diffraction by ultrashort waves, Izvest. Akad. Nauk S.S.S.R. Ser. Fiz. No. 2 (1937).

[28] J. Feinstein, Some stochastic problems in wave propagation—Part II, IRE Trans. **AP-2,** 63, (1954).

[29] R. B. Muchmore, and A. D. Wheelon, Line-of-sight propagation phenomenon, I Proc. I.R.E. **43,** 1437 (1955).

[30] J. W. Herbstreit, et al., Radio studies of atmospheric turbulence, vol. I and II, May 31, 1956 (to be published).

[31] E. Levin, R. B. Muchmore and A. D. Wheelon. Aperature-to-medium coupling on line-of-sight paths: Fresnel scattering, to be published in IRE Trans. PGAP (1959).

[32] K. A. Norton, P. L. Rice, H. B. Janes and A. P. Barsis, The rate of fading in propagation through a turbulent atmosphere, Proc. I.R.E. **43,** 1341 (1955).

[33] J. W. Herbstreit, and M. C. Thompson. Measurements of the phase of radio waves received over transmission paths with electrical lengths varying as a result of atmospheric turbulence, Proc. I.R.E. **43,** 1391 (1955).

[34] A. P. Dean, and B. M. Fannin, Phase difference variations in 9350 mc radio signals arriving at spaced antennas, Proc. I.R.E. **43,** 1402 (1955).

[35] E. Barrows, Effect of tropospheric fluctuations on radio star signals, to be submitted for publication to J. Research NBS, Section D (Radio Propagation).

[36] V. A. Krasil'nikov, The effect of variations of the coefficient of refraction in the atmosphere upon the propagation of ultrashort radio waves, Izvest. Akad. Nauk. S.S.S.R. Sev. Geograf i Geofiz **13,** 33 (1949).

[37] P. G. Bergman, Propagation of radiation in a medium with random inhomogeneities, Phys. Rev. **70,** 486 (1946).

[38] E. C. S. Megaw, Interpretation of stellar scintillation, Quart. J. Royal Meteorol. Soc. **80,** 248 (1954).

[39] A. M. Obukhov, On the effect of weak atmospheric inhomogeneities on sound and light propagation, Izvest. Akad. Nauk. S.S.S.R. Ser. Geofiz. No. 2, 155 (1953).

[40] L. A. Chernov, Correlation of the amplitude and phase fluctuations in wave propagation in media with random inhomogeneities, Akusticheskii Zhurnal **1,** 89 (1955) and A. N. Doklady, USSR **98,** 953 (1954).

[41] V. I. Tatarskii, On the theory of the propagation of sound waves in a turbulent stream, Zhur. Eksptl'i i Theoret Fiz. **25,** 74 (1953).

[42] B. M. Fannin, Line-of-sight wave propagation in a randomly inhomogeneous medium, IRE Trans. PGAP, **AP–4,** 661 (1956).

[43] R. P. Feynman, Space-time approach to quantum electrodynamics, Phys. Rev. **76,** 769 (1949).

[44] R. B. Muchmore, and A. D. Wheelon, Line-of-sight propagation phenomenon II, Proc. I.R.E. **43,** 1437 (1955).

[45] C. L. Pekeris, Note on the scattering of radiation in an inhomogenous medium, Phys. Rev. **71,** 268 (1947).

[46] H. G. Booker, and W. E. Gordon, A theory of radio scattering in the troposphere, Proc. I.R.E. **38,** 401 (1950).

[47] See papers in the Scatter Prop. Issue, Proc. I.R.E. **43** (Oct. 1955).

[48] K. Bullington, Characteristics of beyond-the-horizon radio transmission, Proc. I.R.E. **43,** 1175 (1955).

[49] H. Staras, and A. D. Wheelon, Theoretical research on tropospheric scatter propagation in the United States 1954–1957, IRE Trans. PGAP **AP–7,** 80 (1959).

[50] R. A. Silverman, Some remarks on scattering from eddies, Proc. I.R.E. **43,** 1253 (1955).
[51] M. Balser, and R. A. Silverman, Statistics of electromagnetic radiation scattered by a turbulent medium, Phys. Rev. **96,** 960 (1954).
[52] H. B. Janes, An analysis of within-the-hour fading in 100-to-1000-Mc transmissions, J. Research NBS **54,** 231 (1955) RP 2585.
[53] A. P. Barsis, J. W. Herbstreit and K. O. Hornberg, Cheyenne Mountain tropospheric propagation experiments, NBS Circ. 554 (1955).
[54] G. McCrossen, Analysis of the long term distribution of instantaneous received power (to be published).
[55] L. D. Arons, An analysis of radio-wave scattering in the diffraction region, Cornell Univ. E. E. Report 312 (30 Oct. 1956, Ithaca, N.Y.).
[56] H. Bremmer, Terrestial Radio Waves (Elsevier Press, Inc., Houston, Texas, 1949).
[57] H. Feshbach, Unpublished Lincoln Laboratory Memoranda.
[58] K. A. Norton, P. L. Rice, and L. E. Vogler. The use of angular distance in estimating transmission loss and fading range for propagation through a turbulent atmosphere over irregular terrain, Proc. I.R.E. **43,** 1488 (1955).
[59] J. H. Chrisholm, P. A. Portmann, J. T. deBettencourt, and J. F. Roche, Investigations of angular scattering and multipath properties of tropospheric propagation of short radio waves beyond the horizon, Proc. I.R.E. **43,** 1317 (1955).
[60] B. R. Bean, and R. Abbott. Oxygen and H_2O vapor absorption of radio waves in the atmosphere, Geofis pura e appl, **37,** 127 (1957).
[61] R. L. Abbott, unpublished work.
[62] P. L. Rice, A. G. Longley, and K. A. Norton, Prediction of the cumulative distribution with time of ground wave and tropospheric wave transmission loss, NBS Technical Note 15 (July 1959).
[63] W. E. Gordon, Radio Scattering in the Troposphere, Proc. I.R.E. **43,** 25 (1955).
[64] H. Staras, Forward scattering of radio waves by anisotropic turbulence, Proc. I.R.E. **43,** 1374 (1955).
[65] T. F. Rogers, VHF field strength far beyond the radio horizon, Proc. I.R.E. **43,** 623 (1955).
[66] J. W. Herbstreit, K. A. Norton, P. L. Rice, and G. E. Schafer, Antennas and propagation, IRE Convention Record, Part 2, pp. 85–93 (March 1953).
67] A. T. Waterman, Some generalized scattering relationships in transhorizon propagation, Proc. I.R.E. **46,** 1842 (1958).
[68] S. O. Rice, Statistical fluctuations of radio field strength far beyond the horizon, Proc. IRE **41,** 274 (1953).
[69] J. B. McGuire, and A. D. Wheelon, Calculation of the fading rate for tropospheric scatter propagation, Presented at spring URSI Meeting, Washington, D.C. (1958).
[70] V. I. Bunimovich, Fluctuating processes as oscillations with random amplitudes and phases, Zhur. Tekh. Fiz. **19,** 1231 (1949).
[71] C. L. Mack, Diversity Reception in UHF Long Range Communications, Proc. I.R.E. **43,** 1281 (1955).
[72] A. F. Barghausen, M. T. Decker, and L. J. Maloney, Measurements of correlation, height gain, and path antenna gain at 1046 Mc on spaced antennas far beyond the radio horizon, 1955 IRE Convention Record, Part I, Vol. 3.
[73] H. Staras, Diversity reception with correlated signals, J. Appl. Phy. **27,** 93 (1956), see also Proc. I.R.E. **44,** 1057 (1956).
[74] R.C.A. Report, Study and investigation of tropospheric scattering, Part A, **91** (1956), per U.S. Army Signal Corps Eng. Labs, Contract DA–36–039–SC–64555.
[75] H. B. Janes and P. I. Wells, Some tropospheric scatter propagation measurements near the horizon, Proc. I.R.E., **43,** 1336 (1955).
[76] H. G. Booker and J. T. de Bettencourt, Theory of radio transmission by tropospheric scattering using very narrow beams, Proc. IRE, **43,** 281 (1955).
[77] J. H. Chisholm, L. P. Rainville, J. F. Roche, and H. G. Root, Measurements of the bandwidth of radio waves propagated by the troposphere beyond the horizon, IRE Trans. PGAP, **AP–6,** 377 (1958).
[78] W. H. Tidd, Demonstration of bandwidth capabilities of beyond-the-horizon tropospheric radio propagation, Proc. IRE., **43,** 1297 (1955).
[79] H. Staras, Antenna-to-medium coupling loss, IRE Trans. PGAP, **AP–5,** 288 (1957).
[80] W. Hartman and R. Wilkerson, Path antenna gain in an exponential atmosphere, to be published in J. Research NBS, 63D (Nov. 1959).
[81] D. K. Bailey, R. Bateman, and R. C. Kirby, Radio transmission at VHF by scattering and other processes in the lower ionosphere, Proc. IRE, **43,** 1181 (1955).

BOULDER, COLO. (Paper 63D2–19.)